Remote Sensing of Environment 216 (2018) 212–229

Contents lists available at ScienceDirect

Remote Sensing of Environment

journal homepage: www.elsevier.com/locate/rse

Generation and evaluation of the VIIRS land surface phenology product

Xiaoyang Zhang[a,b,*], Lingling Liu[a], Yan Liu[e], Senthilnath Jayavelu[a], Jianmin Wang[a], Minkyu Moon[d], Geoffrey M. Henebry[a,c], Mark A. Friedl[d], Crystal B. Schaaf[e]

[a] Geospatial Sciences Center of Excellence, South Dakota State University, Brookings, SD 57007, USA
[b] Department of Geography, South Dakota State University, Brookings, SD 57007, USA
[c] Department of Natural Resource Management, South Dakota State University, Brookings, SD 57007, USA
[d] Department of Earth and Environment, Boston University, Boston, MA 02215, USA
[e] School for the Environment, University of Massachusetts Boston, Boston, MA 02125, USA

ARTICLE INFO

Keywords:
Land surface phenology
VIIRS time series
Phenology product
Evaluation and validation

ABSTRACT

Vegetation phenology is widely acknowledged to be a sensitive indicator of the response of ecosystems to climate change, and phenological shifts have been shown to exert substantial impacts on ecosystem function, biodiversity, and carbon budgets at multiple scales. Therefore, long-term records of the phenology of the vegetated land surface are critical in exploring the biological response to environmental change at regional to global scales. Land surface phenology (LSP) from satellite observations has been extensively used to monitor the dynamics of terrestrial ecosystems in the face of a changing climate. Here we introduce and describe the global land surface phenology (GLSP) product derived from the Visible Infrared Imaging Radiometer Suite (VIIRS) data at a gridded spatial resolution of 500 m. This new product will provide continuity for the Moderate Resolution Imaging Spectroradiometer (MODIS) GLSP product that has been produced on an operational basis since 2001. The VIIRS GLSP algorithm uses daily VIIRS Nadir BRDF (Bidirectional Reflectance Distribution Function)-Adjusted Reflectance (NBAR) data as the primary input to calculate the two-band enhanced vegetation index (EVI2) at each 500 m pixel. The temporal EVI2 trajectory is modeled using a hybrid piecewise logistic function to track the seasonal vegetation development, detect phenological transition dates, calculate the magnitude of vegetation greenness development, and characterize the confidence of phenology detections. The VIIRS GLSP algorithm has been implemented across the contiguous United States, and the resulting phenological metrics have been evaluated through comparisons with species-specific field phenological observations, Landsat phenology retrievals, and the MODIS phenology detections. The results demonstrate that the VIIRS GLSP metrics are of high quality and are in a good agreement with the other independent satellite and field observations. The results also indicate that the uncertainty in the VIIRS GLSP retrievals is primarily associated with missing high quality observations in VIIRS EVI2 time series.

1. Introduction

Vegetation phenology can be a sensitive indicator of biological responses to environmental change (Cleland et al., 2012; Ivits et al., 2012; Morisette et al., 2009). Long-term records of vegetation phenology, observed from both species-specific in situ data and satellite observations, have been used to explore the dynamics of biospheric processes at regional to global scales (Cleland et al., 2007; Korner and Basler, 2010; Parmesan and Yohe, 2003; Richardson et al., 2013; Walther, 2010). Because vegetation phenology is a parameter that is readily observable and easily understood by the public, it is widely acknowledged to be a key indicator that can be used to track ecosystem responses to climate change by the Intergovernmental Panel on Climate Change (IPCC, 2007, 2014), the United States Global Change Research Program (USGCRP, 2010, 2015), and the Environmental Protection Agency (EPA, 2016).

The phenological dynamics of vegetation influence a host of ecophysiological processes including hydrological processes (Gerten et al., 2004; Hogg et al., 2000; Vivoni, 2012), biogeochemistry and nutrient cycling (Campbell et al., 2009; Cooke and Weih, 2005), land-atmosphere interactions (Heimann et al., 1998; Puma et al., 2013), and terrestrial carbon cycling across a wide range of ecosystem and climatic regimes (Baldocchi et al., 2001; Churkina et al., 2005; Gray et al., 2014; Richardson et al., 2009). The presence and absence of foliage affects land surface albedo (Moore et al., 1996; Ollinger et al., 2008; Wang et al., 2017; Williamson et al., 2016), and exerts strong controls on

* Corresponding author at: Geospatial Sciences Center of Excellence, South Dakota State University, Brookings, SD 57007, USA.
E-mail address: xiaoyang.zhang@sdstate.edu (X. Zhang).

https://doi.org/10.1016/j.rse.2018.06.047
Received 30 March 2018; Received in revised form 27 June 2018; Accepted 28 June 2018
Available online 11 July 2018
0034-4257/ © 2018 Elsevier Inc. All rights reserved.

surface radiation budgets and the partitioning of net radiation between latent and sensible heat fluxes (Chen and Dudhia, 2001; Vivoni, 2012). Therefore, accurate and timely information related to the spatio-temporal dynamics of vegetation phenology is required for investigations focused on monitoring climate change and modeling biospheric processes. While some data sets related to the phenology of particular plant species have been collected at specific sites and across networks, remote sensing provides the only realistic way to observe and monitor phenological dynamics and changes at landscape to global scales on a systematic basis.

Phenological metrics characterizing seasonality in the vegetated land surface have been widely observed from remotely sensed data at regional to global scales over the past three decades. To distinguish these metrics from direct measurements of plant phenology collected on the ground, remote sensing-based observations of phenology are generally referred to as land surface phenology (LSP) (de Beurs and Henebry, 2004; Friedl et al., 2006; Henebry and de Beurs, 2013). Satellite remote sensing data at a moderate spatial resolution provide global daily measurements of land surface properties, and therefore are well-suited for monitoring the seasonal patterns and trends due to regional to global phenological variation and change (de Beurs and Henebry, 2005; Henebry and de Beurs, 2013; Reed et al., 1994; White et al., 1997; Zhang et al., 2003; Zhang et al., 2014). As a result, exploiting the growing archive of global optical satellite data, such as the Advanced Very High Resolution Radiometer (AVHRR), the Moderate Resolution Imaging Spectroradiometer (MODIS), and SPOT-VEGETATION, a number of algorithms have been developed to detect LSP at regional and global scales. These algorithms rely on a time series of vegetation indices (VI) that are smoothed to reduce noise in weekly to biweekly values. The most commonly used smoothing methods include moving-window averages (Reed et al., 1994), Fourier harmonic analyses (Moody and Johnson, 2001), asymmetric Gaussian function-fits (Jonsson and Eklundh, 2002), piece-wise logistic functions (Zhang et al., 2003), Savitzky–Golay filters (Chen et al., 2004), quadratic models based on degree-day accumulations (de Beurs and Henebry, 2004; Henebry and de Beurs, 2013), and polynomial curve fitting (Bradley et al., 2007). Smoothed VI time series are then used to detect phenological metrics based on a wide array of methods that identify the timing of the start and end of a vegetation growing season, including threshold-based techniques (Jonsson and Eklundh, 2002; White et al., 1997), harmonic analyses (Jakubauskas et al., 2001; Moody and Johnson, 2001), and inflection point estimates within the time series of vegetation indices (Moulin et al., 1997; Zhang et al., 2003). However, considerable differences still exist among the various phenological detection methods (de Beurs and Henebry, 2010; White et al., 2009).

Although a great number of LSP products have been developed using different methods and satellite observations, most of them have been produced for specific regions and time periods for specific research purposes. To date, the MODIS Land Cover Dynamics Product (MCD12Q2) is the only global land surface phenology (GLSP) product that is produced on an operational basis from 2001 to present (Ganguly et al., 2010; Zhang et al., 2006; Zhang et al., 2003), and is publically accessible (https://lpdaac.usgs.gov/dataset_discovery/MCD12Q2). This product (MCD12Q2) employs MODIS enhanced vegetation index (EVI) data, computed from the MODIS nadir bidirectional reflectance distribution function (BRDF)-adjusted reflectance (NBAR) data (Schaaf et al., 2002) to generate 500 m gridded phenological metrics on an annual basis (Ganguly et al., 2010).

As the MODIS sensors on both Terra and Aqua are aging and nearing the end of their duty cycles (expected to continue operating through early 2020s), the Visible Infrared Imaging Radiometer Suite (VIIRS), launched on the Suomi National Polar-orbiting Partnership (NPP) platform in October 2011, is being used to continue the record of measurement provided by the MODIS instruments (Goldberg et al., 2013; Justice et al., 2013). The VIIRS instrument represents a new generation of moderate-resolution imaging radiometer that follows the legacy of the MODIS and AVHRR sensors (Justice et al., 2013; Román et al. 2012). In support of this, an operational VIIRS product is being implemented to continuously monitor the dynamics of global land surface phenology and to establish a long-term phenological data record for the post-MODIS era. This product will provide consistent spatial and temporal estimates of the timing and magnitude of vegetation phenological development across the globe, and will be suitable for characterizing and understanding interannual-to-decadal scale ecosystem variation in response to environmental change. This paper provides an overview of the 500 m VIIRS GLSP product generation, including the algorithm development and product evaluation.

2. Algorithms for the VIIRS GLSP

The VIIRS GLSP algorithm is based on the heritage of the MODIS land cover dynamics (MLCD12Q2) algorithm in collection 5 (Ganguly et al., 2010). Although the details of the MODIS GLSP have been described elsewhere (Zhang, 2015; Zhang et al., 2006; Zhang et al., 2003), the VIIRS algorithm is different in several important elements, and so here we provide a brief description of the algorithm used specifically for the generation of VIIRS GLSP product.

2.1. Input data

The primary input will be the daily 500 m VIIRS BRDF NBAR product (VNP43IA4). Daily NBAR values are produced utilizing all high-quality, cloud-cleared, and atmospherically-corrected surface reflectance available over a 16-day moving window to identify the best fit parameters for the Ross-Thick/Li-Sparse-Reciprocal (RTLSR) semi-empirical BRDF model (Liu et al., 2017c; Schaaf et al., 2002; Schaaf et al., 2011; Wang et al., 2018; Wang et al., 2012). The daily retrieved BRDF model parameters are used to correct the reflectance variations resulting from off-nadir viewing geometry and to adjust the solar zenith angle to local solar noon. The NBAR product also provides quality assurance (QA) flags, including the retrieval quality (high quality – NBAR retrieval from the full inversion model; low quality - NBAR retrieval from the back up magnitude inversion model; and fill values - no surface retrievals because of cloud cover or a lack of VIIRS observations) (Liu et al., 2017b). The presence of snow in the NBAR data is flagged in the VIIRS BRDF\Albedo\NBAR Quality Assurance product (VNP43IA2).

To evaluate the VIIRS GLSP product, this study uses 14 tiles of VIIRS NBAR data and the corresponding QA product (VNP43IA4 and VNP43IA2) that were generated offline while the operational VIIRS BRDF/Albedo/NBAR products will be released through NASA in late 2018. These tiles (h08v04, h08v05, h08v06, h09v04, h09v05, h09v06, h10v04, h10v05, h10v06, h11v04, h11v05, h12v04, h12v05 and h13h04) cover the entire CONtiguous United States (CONUS), southern Canada, and northern Mexico. The data collected ranged from July 2012 to June 2015 and were used to detect phenological metrics for 2013 and 2014.

Ancillary data used by the algorithm will include VIIRS land surface temperature (LST) and land cover types. In this study, we use the MODIS land surface temperature product (MOD11A1) from July 2012 to June 2015 and the MODIS 500 m land cover product (MCD12Q1) from 2013 to implement the VIIRS GLSP algorithm, because NASA gridded VIIRS LST product is still under development and there is currently no VIIRS land cover product. The daily 1 km MODIS LST data were resampled to a 500 m grid using a nearest neighbor method to match the spatial resolution of the NBAR data.

2.2. Preprocessing of NBAR time series

The daily two-band enhanced vegetation index (EVI2) will be calculated from the red and near infrared VIIRS NBAR products to track seasonal variation in the vegetated land surface. Note that there is no available blue surface reflectance product to compute a conventional

EVI, but EVI2 has been shown to be functionally equivalent to EVI (Huete et al., 2006; Jiang et al., 2008), and has several advantages over the NDVI which is most commonly used for monitoring vegetation. Specifically, EVI2 is less prone to saturation over dense vegetation cover and is less sensitive to different background soil reflectances and non-green winter land surfaces (Huete et al., 2006; Jiang et al., 2008; Rocha and Shaver, 2009). Moreover, phenological metrics detected from the EVI2 time series are more comparable to in situ PhenoCam observations than those from satellite based NDVI values (Klosterman et al., 2014). To reduce the data volumes, while still retaining fine temporal resolution, and to increase processing speed, daily NBAR EVI2 values will be aggregated to 3-day composites by first selecting the best quality data within each 3-day window and selecting the maximum value composite if more than one value is available in each 3-day period. In parallel, the corresponding NDVI values are also recorded to identify anomalously large EVI2 (see below).

Unusually large EVI2 values can arise from spuriously low red band values caused by an inaccurate atmospheric correction or a variety of other factors. To exclude these cases, anomalous EVI2 values are identified as EVI2 values that are larger than 90% of the corresponding NDVI values, or that are larger than 110% of any EVI2 values generated during the previous and succeeding one-month periods. These thresholds were determined from a comparison of MODIS NDVI and EVI2 time series across the globe. When such anomalous values are identified, they are treated as fill values.

To remove the effect of snow on the EVI2 data, the algorithm identifies the minimum snow-free EVI2 value (hereafter, "the background EVI2") for each pixel based on a two-year window that includes the preceding half-year, the current year, and the subsequent half-year. The background EVI2 value represents the minimum EVI2 of the soil and vegetation mixture in an annual time series (Zhang, 2015; Zhang et al., 2007). Assuming that vegetation is dormant during the winter (or wherever the surface has daytime LST < 278 K), the maximum EVI2 value during the dormant phase reflects the snow-free surface background condition before the onset of the growing season. However, reliable EVI2 values during winter are not always obtained from any given two-year period, as there may be no cloud- and snow- free observations available. Thus, the candidate background EVI2 values are first determined using: (1) the mean of the 50% largest cloud- and snow-free winter EVI2 values, where the winter period is determined based on LST < 278 K, or (2) the mean of the 10% smallest cloud-free EVI2 values during periods where LST > 278 K appears during the two-year window. If both cases occur, the average of these two candidate values is used as the background value. Otherwise, the latter is selected if high quality EVI2 values during winter are not available. Note that the LST is only used to identify the time period when irregular EVI2 values are contaminated by residual snow or partial snow cover (including under-canopy snow), rather than to determine an exact winter period by date.

The resulting VIIRS EVI2 time series over each two-year window will be then smoothed to further reduce any remaining noise. Persistent cloud cover is the major issue that causes missing data in the VIIRS NBAR product, and significantly reduces the numbers of observations and quality of EVI2 time series. Such fill values in the EVI2 time series are replaced using the moving average of the two neighboring high quality values starting from the point closest to the larger EVI2 values.

Spurious phenology cycles in EVI2 time series, which frequently arise because of variation caused by residual unscreened cloud influences in periods of persistent cloud contamination, will be removed depending on the land cover type. Specifically, it is assumed that two vegetation growing peaks (cycles) do not occur within six months in forest land cover types or within two months in shrublands, grasslands, and croplands. Where detected, these spurious cycles are flagged, and associated EVI2 values are replaced using a moving average of the two neighboring high quality values. Finally, after cloud-contaminated values are replaced, Savitzky-Golay filters will be applied to further ameliorate irregular variations in the EVI2 time series.

2.3. Detection of phenological metrics

Greenup and senescence phases of vegetation growth cycles will be identified from the smoothed EVI2 time series. These phases represent periods at each pixel with sustained EVI2 increase or decrease, where transitions from periods of increasing (decreasing) EVI2 to periods of decreasing (increasing) EVI2 are identified by changes from positive to negative slope over five-point moving windows. Short periods with slight decreases or increases in EVI2 that result from transient processes unrelated to vegetation cycles could still retain in some cases after preprocessing in Section 2.2. These short periods are only removed if the ratio of the local maximum EVI2 to the annual maximum EVI2 is < 0.25. This approach screens out short-term variations unrelated to growth and senescence cycles, while allowing multiple growth cycles within any 12-month period to be retained.

A hybrid piecewise logistic model (HPLM) will be applied to the times series to model each EVI2 increasing or decreasing phase in a vegetation growth cycle. The HPLM accommodates EVI2 trajectories that are associated with both favorable conditions and stressed conditions in vegetation growth using the following formula (Zhang, 2015):

$$EVI2(t) = \begin{cases} \frac{c_1}{1+e^{a_1+b_1\times t}} + EVI2_b & \text{Favorable growth condition} \quad (1) \\ \frac{c_2+d\times t}{1+e^{a_2+b_2\times t}} + EVI2_b & \text{Vegetation stress condition} \quad (2) \end{cases}$$

where t is time in the day of year (DOY), a is related to the vegetation growth period, b is associated with the rate of plant leaf development, c is the amplitude of EVI2 variation, d is a vegetation stress factor (Elmore et al., 2012; Melaas et al., 2013), and $EVI2_b$ is the background (dormant season) value. In order to determine whether the plant suffers from stress or not, the time series fit to Eqs. (1) and (2) are compared using an index of agreement described in Section 2.4 (Eq. (5)), and the function with the better fit is selected.

From the fitted HPLM models, the curvature $K_{(t)}$ and curvature change rate $K_{(t)}'$ are calculated to identify distinct phenological transition dates that correspond to a day-of-year (DOY) (Zhang et al., 2003):

$$K_{(t)} = \frac{d\alpha}{ds} = \frac{EVI2_{(t)}''}{(1+EVI2_{(t)}'^2)^{\frac{3}{2}}} \quad (3)$$

$$K_{(t)}' = \frac{dK_{(t)}}{dt} \quad (4)$$

where α is the angle (in radians) of the unit tangent vector at time t along a differential curve, s is the unit length of the curve, and $EVI2_{(t)}'$ and $EVI2_{(t)}''$ are the first and second derivatives of $EVI2_{(t)}$, respectively.

Based on the HPLM (Eqs. (1) and (2)) and the curvature change rate (Eq. (4)), a set of phenological metrics in the VIIRS GLSP product will be identified. During a vegetation growth period, when vegetation transitions from a dormant phase to a greenup phase, three extreme points are identified along $K_{(t)}'$. Two maximum and one minimum values correspond, respectively, to the following phenological transition dates: (1) greenup onset (the date of onset of EVI2 increase), (2) maturity onset (the date of onset of EVI2 maximum), and (3) date at mid-greenup phase. During a senescence period, when vegetation transitions from the maturity phase to a senescence phase, three extreme points (two minimum and one maximum values) are used to identify transition dates: (4) senescence onset (the date of onset of EVI2 decrease), (5) dormancy onset (the date of onset of EVI2 minimum), and (6) date at mid-senescent phase. In addition, the VIIRS GLSP algorithm also retains the EVI2 values at the greenup onset and maturity onset.

2.4. VIIRS GLSP quality assurance

Quality assurance (QA) information is included in the VIIRS GLSP

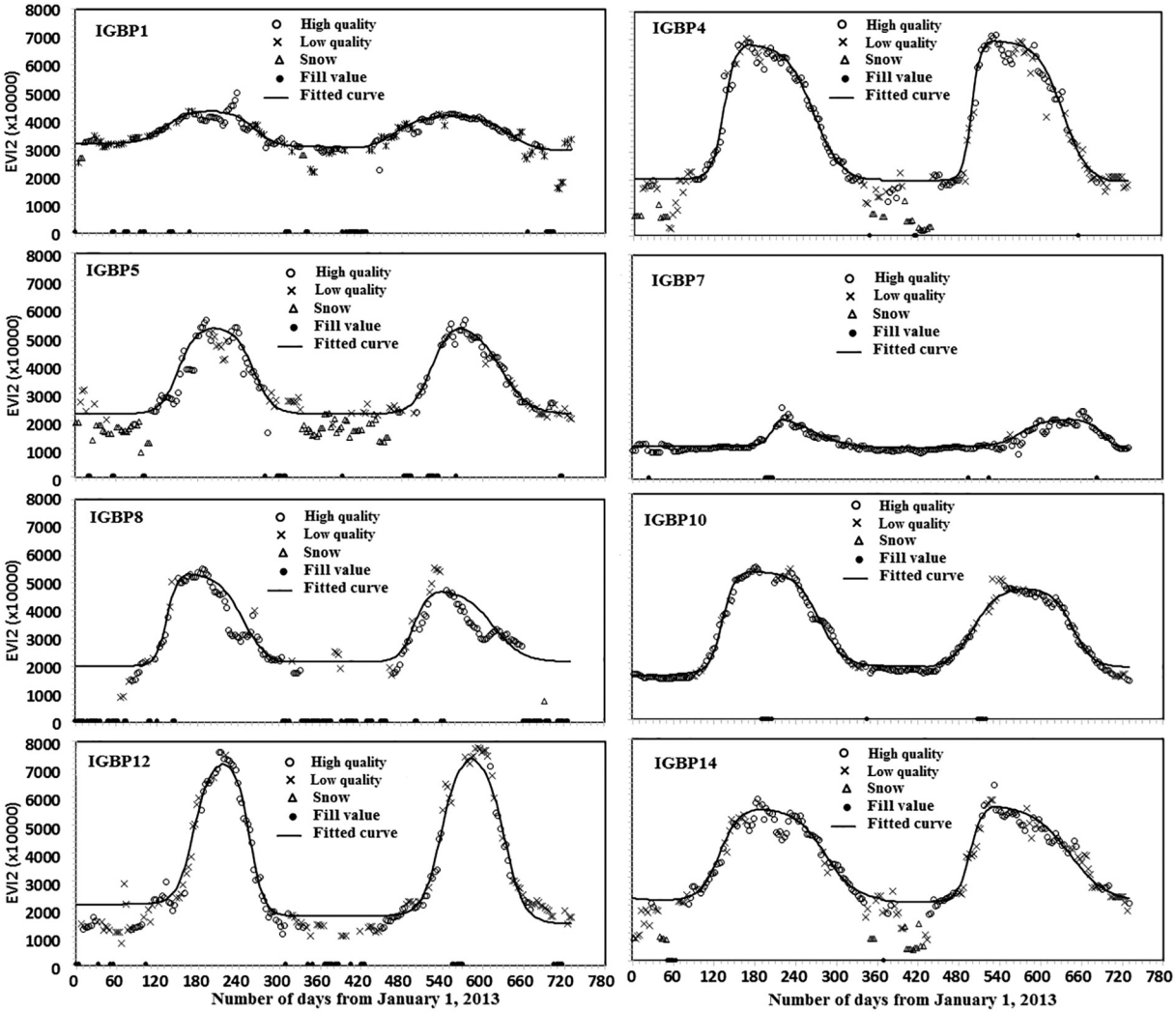

Fig. 1. Time series of VIIRS NBAR EVI2 data and HPLM-modeled curves for several randomly selected IGBP land cover types during 2013–2014. IGBP1-evergreen needleleaf forest, IGBP4-deciduous broadleaf forest, IGBP5-mixed forest, IGBP7-open shrublands, IGBP8-woody savanna, IGBP10-graslands, IGBP12-croplands, and IGBP14-cropland/natural vegetation mosaic.

product. To this end, information related to the HPLM model fit and the proportion of high quality data in a EVI2 time series will be employed to quantify the relative quality of the GLSP metrics at each pixel. The goodness of fit characterizes discrepancies between the HPLM modeled values and the high quality VIIRS NBAR EVI2 observations from greenup onset to dormancy onset at each pixel using an agreement index (AI) (Willmott, 1981; Zhang, 2015):

$$AI = 100 - 100\frac{\sum_{i=1}^{n}(P_{(i)} - O_{(i)})^2}{\sum_{i=1}^{n}(|P_{(i)} - \overline{O}| + |O_{(i)} - \overline{O}|)^2} \quad (5)$$

where n is the number of VIIRS NBAR observations with high quality, $P_{(i)}$ is the HPLM modeled value at i^{th} observation, $O_{(i)}$ is the EVI2 value with high quality, and $\bar{O}$ is the mean EVI2 with high quality during a vegetation growing season.

The agreement index (AI) provides a measure of the relative error in model estimates at each pixel. It is dimensionless and ranges from 0 (complete disagreement) to 100 (perfect fit). The AI is also sensitive to differences between observed and modeled means (Willmott, 1981). Thus, the AI is comparable across different biomes and climates.

The quality of the fitted HPLM model at each pixel is strongly dependent on the number of high quality observations (Zhang et al., 2009). Accordingly, the proportion of high quality (PHQ) EVI2 values during a vegetation growing season for a given pixel is included in the quality assurance data for that pixel. Based on a sensitivity analysis, the error in vegetation phenology detection using logistic models is minimized if the temporal resolution of the vegetation index is finer than 8 days (Zhang et al., 2009). In other words, vegetation temporal trajectories can be realistically reconstructed if there is at least one high quality EVI2 observation within each 8-day period during the vegetation growing season. In the VIIRS GLSP algorithm, the quality of observations during each growing season at each pixel is calculated as:

$$P_{hq} = \frac{N_{hq}}{T} \times 100 \quad (6)$$

where P_{hq} is the proportion of high quality observations (ranging from 0 to 100), T is the total number of 3-day EVI2 during a growing season, and N_{hq} is the number of three 3-day moving windows that contain high quality observations.

Because the four key phenological transition dates (greenup onset, maturity onset, senescence onset, and dormancy onset) are the most important metrics provided in the phenological product, a confidence metric for each phenological transition date is also included in the VIIRS GLSP product. Specifically, the local EVI2 quality around each phenological transition date is used to describe the confidence for the corresponding phenological transition date detection. The local EVI2

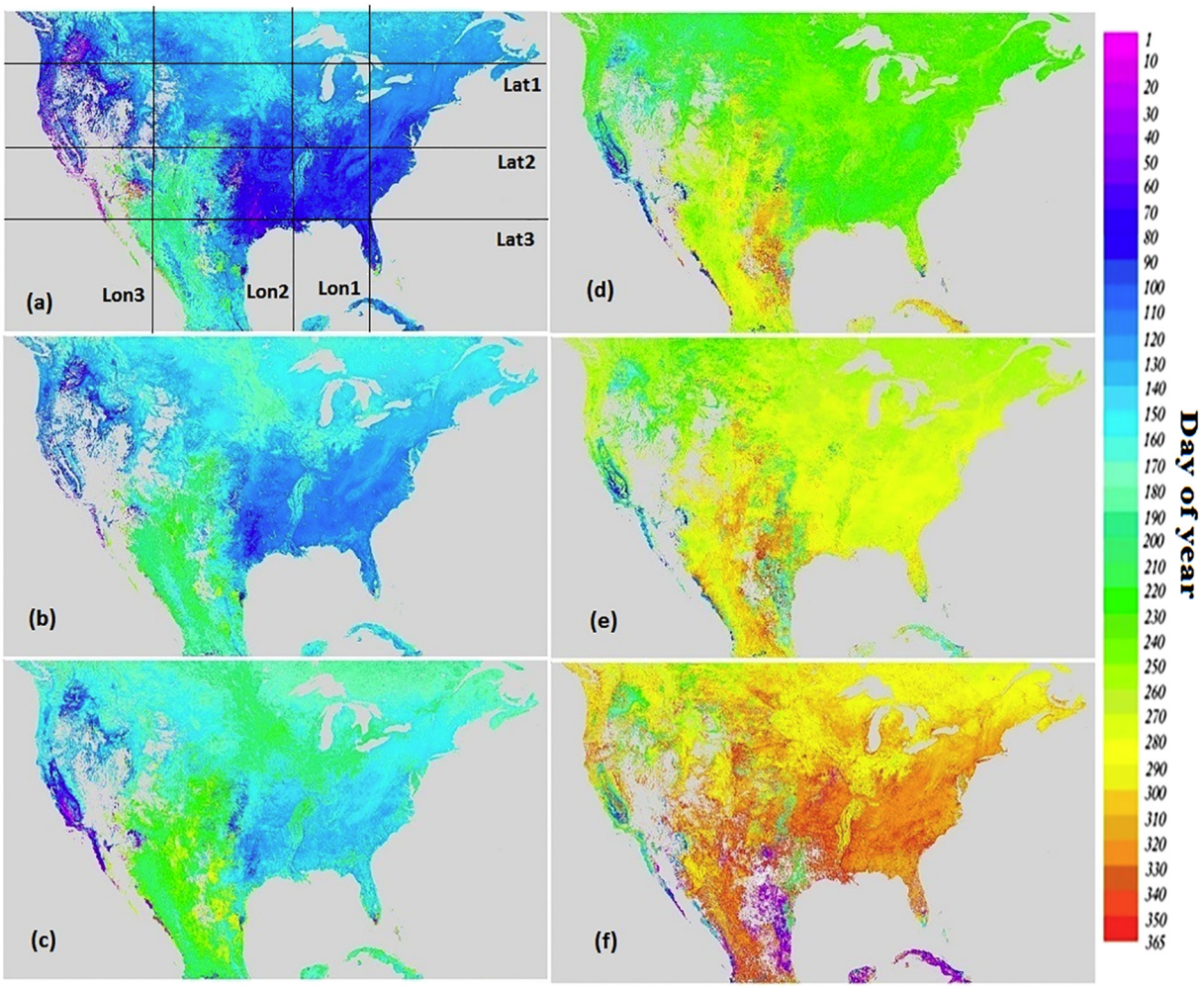

Fig. 2. Phenological transition dates in the VIIRS GLSP detection for 2013 (geographic projection). (a) Timing of greenup onset, (b) mid-date of greenup phase, (c) timing of maturity onset, (d) timing of senescence onset, (e) mid-date of senescence phase, and (f) timing of dormancy onset. The vertical and horizontal lines in (a) are the locations of phenological profiles described in Fig. 3. The gray color represents either water or arid areas without detectable vegetation growth.

quality is defined as the local proportion of high quality (LPHQ) EVI2 values during the three 3-day periods before and after a specific detected phenological transition date. This period is determined based on a previous sensitivity analysis of phenology date detection (Zhang et al., 2009). Thus, unique LPHQ values are calculated for the greenup onset, maturity onset, senescence onset, and dormancy onset metrics at each pixel.

3. Evaluation of VIIRS GLSP metrics

Evaluation (or validation) of satellite-derived land surface phenology is one of the most critical and challenging tasks. The NASA phenology sub-group suggests to conduct validation activities using sites with detailed spatial and temporal ground phenological observations incorporating multiple resolution scaling opportunities across a distributed range of biomes (https://lpvs.gsfc.nasa.gov/Pheno/Pheno_home.html). To evaluate the VIIRS GSLP metrics, therefore, four datasets from different scales are exploited: (1) species-specific measurements from national phenological networks, (2) observations from higher spatial resolution Lanndsat data, (3) observations from MODIS sensors, (4) near-surface monitoring from PhenoCam. This study investigates first three datasets since the evaluation using PheniCam has been conducted and published (Zhang et al., 2018).

3.1. Comparison with field observations

VIIRS GLSP metrics are evaluated using independent data obtained from the United States of America National Phenology Network (USA-NPN; https://www.usanpn.org). The USA-NPN has developed standardized methods for professionals and volunteers to observe and report on the phenology of plants and animals (Denny et al., 2014; Rosemartin et al., 2015). These phenological observations have been widely used to evaluate remote sensing phenology products and to develop models for predicting the timing of spring leaf emergence (Gerst et al., 2016; Jeong et al., 2013; Melaas et al., 2016; Peng et al., 2017b). Here we utilize observations of the timing of leaf bud break for all individual species reported in the USA-NPN across the CONUS in 2013 and 2014 (which includes observations for horticultural species such as cloned lilacs and honeysuckles). The cloned lilac and honeysuckle observations have been observed over a long period starting as early as the 1950s (Rosemartin et al., 2015), and have also been widely used in the evaluation of satellite phenology detections, trends, and extreme events (Allstadt et al., 2015; Ault et al., 2013; Ault et al., 2015; Zhang et al., 2007). To evaluate the VIIRS GLSP product, species-specific timing of leaf bud break data is compared with greenup onset dates in the VIIRS pixels extracted at locations where the NPN data were collected. If more than one USA-NPN observation is available within a VIIRS pixel, the observations are simply averaged. Finally, the relative difference between VIIRS greenup onset and field observation dates is calculated and

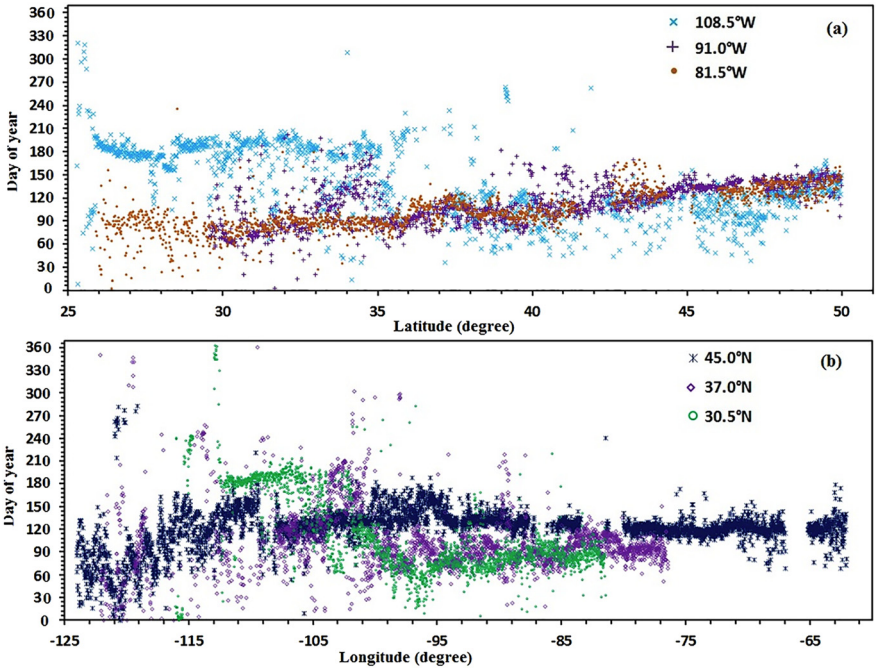

Fig. 3. Profiles of greenup onset along latitude (a) and longitude (b) in 2013. The profiles are defined in Fig. 2: Lat1 = 45.0°N, Lat2 = 37.0°N, Lat3 = 30.5°N, Lon1 = 81.5°W, Lon2 = 91.0°W, and Lon3 = 81.5°W.

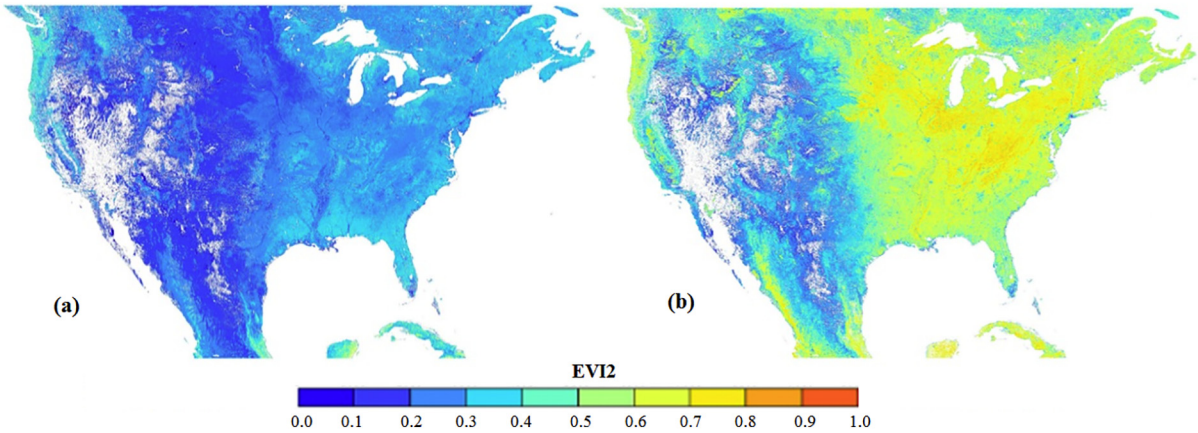

Fig. 4. Spatial distribution of vegetation greenness (EVI2) at greenup onset (a) and at maturity onset (b) in 2013 (geographic projection). The white color represents either water or arid areas without detectable vegetation growth.

their linear correlation is estimated using a geometric mean functional regression (GMFR), a method used for regression analysis that accounts for uncertainty in both the dependent and independent variables.

3.2. Comparison with Landsat phenology detections

VIIRS GLSP product is also evaluated using LSP detections from Landsat data. The USGS (United States Geological Survey) Center for EROS (Earth Resources Observation and Science) generates atmospherically corrected surface reflectance products that are freely accessible from the USGS archive (http://earthexplorer.usgs.gov/). In this study, we detect 30 m phenological dates from Landsat data in two local regions, seperately. First, we utilize atmospherically corrected surface reflectance products from both the Landsat 7 Enhanced Thematic Mapper Plus (ETM+) and Landsat 8 Operational Land Imager (OLI) data in the overlapping zone between path 43/row 33 and path 44/row 33 in 2013, which is located in the Sierra Nevada Mountains, California, with land cover types of oak/grass savanna, open grassland, and mixed forest (Liu et al., 2017a). This dataset includes two Landsat 7 and two Landsat 8 overpasses during each 16-day repeat cycle. Second, we obtain daily fused MODIS – Landsat 8 OLI time series in the central CONUS (Landsat scene of path 26/row 31) in 2013 (Gao et al., 2017), where croplands dominate. The fused time series from Landsat 8 OLI and daily MODIS data provide daily surface reflectance at a spatial resolution of 30 m generated using the STARFM algorithm (Gao et al., 2006). We hereafter refer to these two datasets as the Landsat time series.

Using these Landsat time series, we calculate the EVI2 time series for each region and detect six phenological transition dates using the same approach as for the VIIRS GLSP generation at each 30-m pixel. We then compare the VIIRS phenological dates (500 m) with Landsat phenology detections (30 m) in the relatively homogeneous areas, recognizing that Landsat phenological dates within a heterogeneous VIIRS pixel may vary by as much as three months (Zhang et al., 2017c), which makes it difficult to aggregate 30 m phenological dates to 500 m scales for comparisons. To identify homogeneous pixels, the standard deviation (SD) of the Landsat phenological dates within a VIIRS pixel is calculated, and the SD cumulative frequency distribution is computed

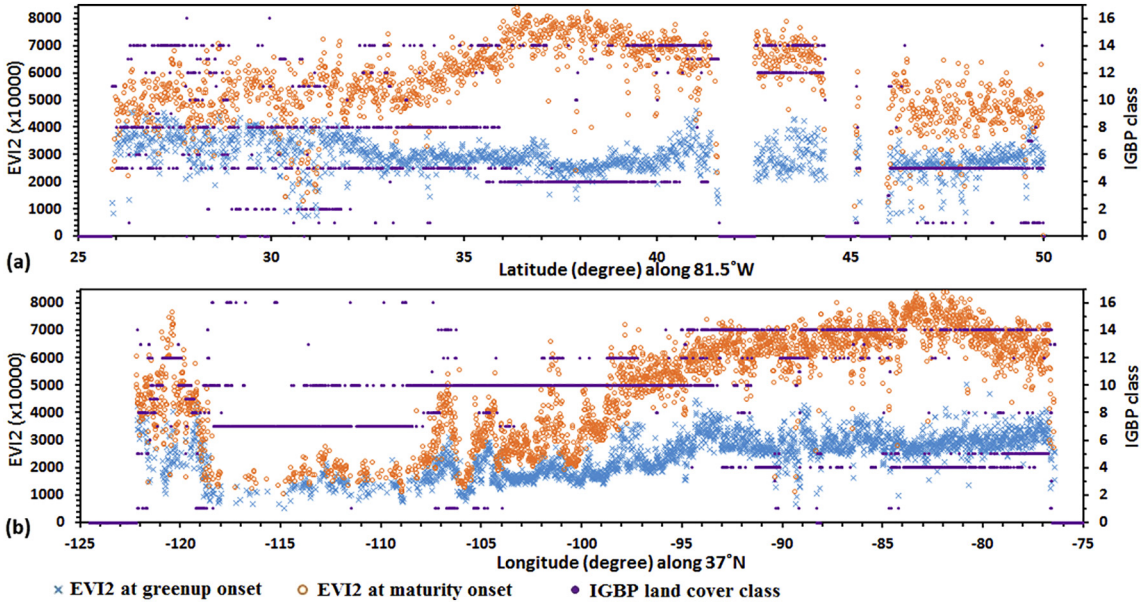

Fig. 5. Variation in the EVI2 greenness at greenup onset and at maturity onset as a function of latitude (a) and longitude (b). The profiles are defined in Fig. 2: Latitude = 37.0°N and Longitude = 81.5°W. The IGBP land cover classes are: 0-water, 1-evergreen needleleaf forest, 2-evergreen broadleaf forest, 3- deciduous needleleaf forest, 4-deciduous broadleaf forest, 5-mixed forest, 6-closed shrublands, 7-open shrublands, 8-woody savanna, 9-savanna, 10-grasslands, 11-permanent wetlands, 12-croplands, 13-urban and built-up areas, 14-cropland/natural vegetation mosaic, 15-snow and Ice, 16-barren or sparsely vegetated.

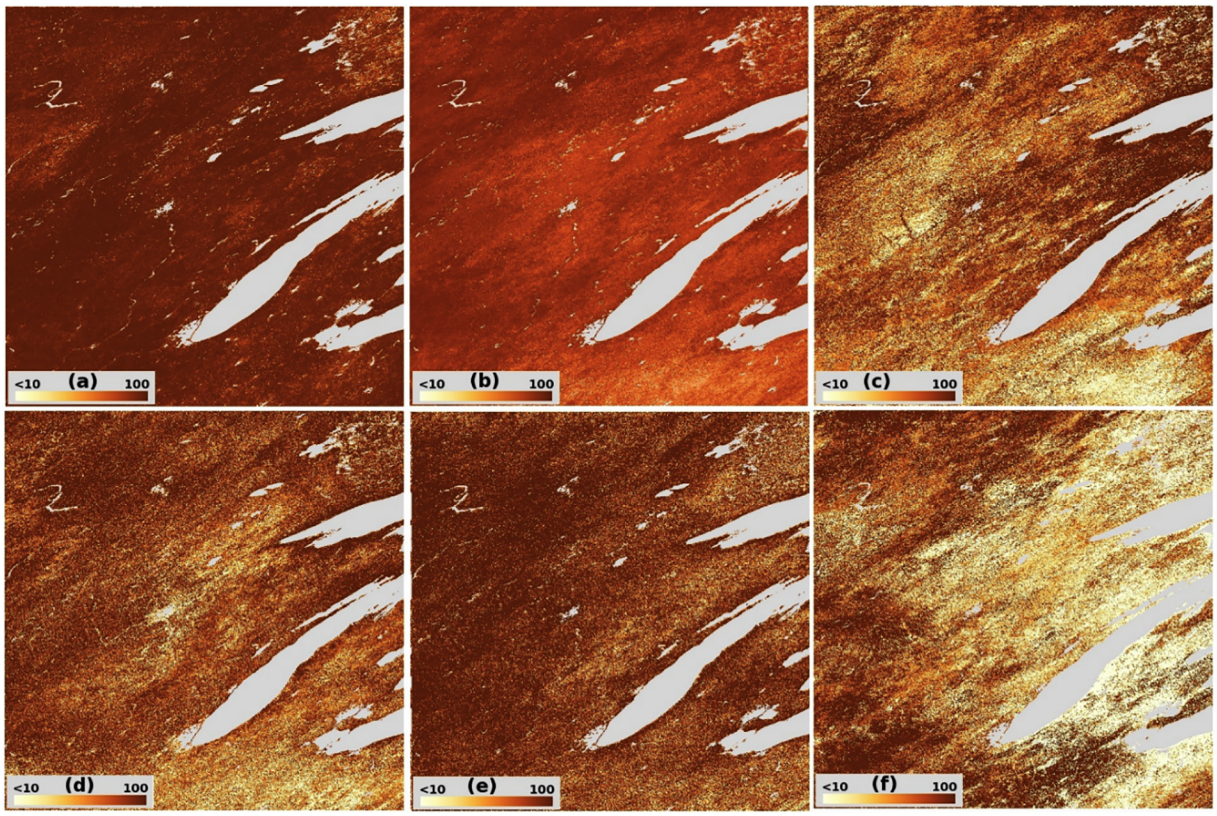

Fig. 6. Spatial variation in the quality of the VIIRS NBAR EVI2 time series (tile h11v04 in sinusoidal projection) in 2013. (a) agreement index (AI), (b) PHQ during the growing season, (c) LPHQ around greenup onset, (d) LPHQ around maturity onset, (e) LPHQ around senescence onset, (f) LPHQ around dormancy onset. The gray pixels are water.

for each Landsat scene. The 20% of the pixels with lowest SD in each region are identified as the most homogeneous pixels. The Landsat phenological dates in these pixels are then used to evaluate each of the six VIIRS phenological dates in the gridded VIIRS pixel by calculating the mean absolute difference (MAD) and the root mean square difference (RMSD).

3.3. Comparison with MODIS phenology values

Intercomparison between the VIIRS and MODIS phenology

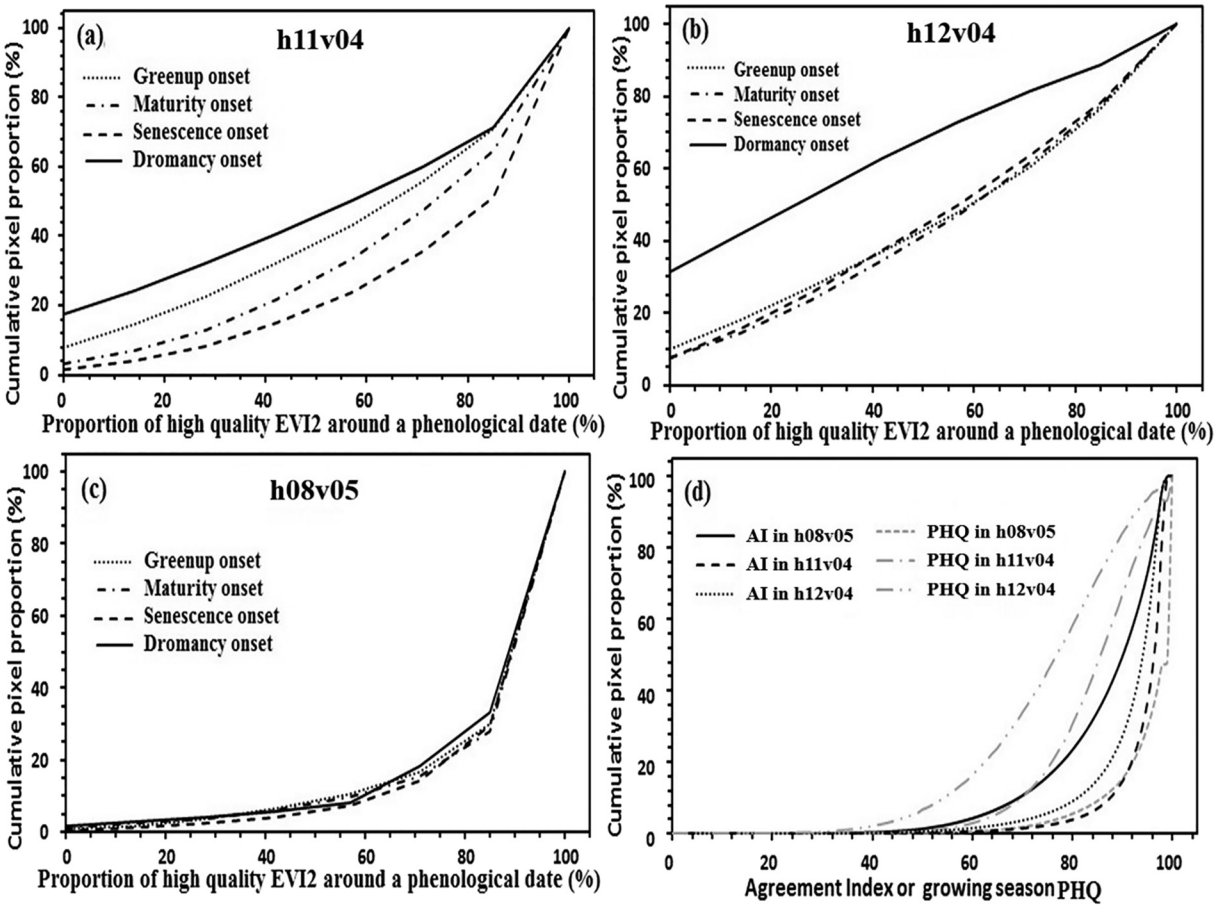

Fig. 7. Cumulative pixel proportion (%) for the average quality of VIIRS EVI2 time series in 2013–2014. (a)–(c) show the local proportion of high quality (LPHQ) values around the greenup onset, maturity onset, senescence onset, and dormancy onset for tiles h11v04, h12v04, and h08v05. (d) indicates the HPLM agreement index and the proportion of high quality (PHQ) EVI2 observations during the vegetation growing season.

detections is performed to characterize and quantify their similarity. This comparison allows us to understand the sources that could cause the differences of phenology detections from VIIRS and MODIS data and generate a consistent long-term environmental data record of GLSP from MODIS and VIIRS. Here we calculate the MODIS phenological metrics using the gridded 500 m MODIS NBAR product (MCD43A4 collection 6) which is produced from a combination of Terra and Aqua MODIS data for tiles of h11v04 (central CONUS), h12v04 (northeastern CONUS), and h08v05 (western CONUS). Although VIIRS and MODIS GLSP products have gridded pixel sizes of 500 m, the effective spatial resolution is closer to 833 m × 618 m for the MODIS NBAR product and 565 m × 595 m in the VIIRS NBAR product (Campagnolo et al., 2016). Therefore, the difference between VIIRS and MODIS phenological dates are compared based on both the raw phenological dates and spatially smoothed values using a 3 × 3 moving window.

Further, we examine the differences in the proportion of high quality observations between the MODIS and VIIRS time series because the quality of the time series is the major source of uncertainty in phenology detections (Zhang et al., 2017b). This difference arises from the fact that MODIS NBAR is produced from both Terra and Aqua MODIS observations while the VIIRS NBAR is produced only from the single NPP VIIRS sensor observations. The impact of EVI2 data quality on phenology detections is investigated using LPHQ in modeling the MODIS and VIIRS time series. Specifically, we stratify the quality of the EVI2 time series into four categories: high quality if the LPHQ = 80–100 occurs in both the MODIS and VIIRS EVI2 datasets, moderate quality if the LPHQ = 40–80, poor quality if the LPHQ = 10–40, and other quality if the LPHQ ≤ 10 or if the LPHQ in both datasets are within different ranges. In each category, the pixel frequency is calculated against the absolute difference of the phenological dates between the MODIS and VIIRS detections. The pixel frequency in the four quality categories is then used to evaluate the impact of the EVI2 quality on phenology detections.

4. Results

4.1. VIIRS EVI2 temporal trajectories in various land cover types

Fig. 1 presents examples of the VIIRS NBAR EVI2 time series during 2013 and 2014, depicting vegetation seasonality across various land cover types. Visual examination indicates that NBAR EVI2 values with high quality (from the full BRDF model) and low quality (from the magnitude BRDF model) track similar seasonal variation in EVI2, although EVI2 values with low quality are more likely to be associated with large uncertainty. The HPLM fits the EVI2 observations well although the EVI2 curves exhibit dissimilar shapes for the different land cover types. The agreement index (AI) between the HPLM modeled values and high quality EVI2 observations for these cases is larger than 90%, indicating the robustness of the HPLM in tracking vegetation seasonality. The AI is larger than 95% for deciduous and mixed forests, croplands, and grasslands, but is lower in shrublands, savannas, and evergreen forests where seasonality in EVI2 is weaker.

4.2. Spatial pattern of VIIRS phenological transition dates

Fig. 2 presents geographic patterns in the six phenological transition

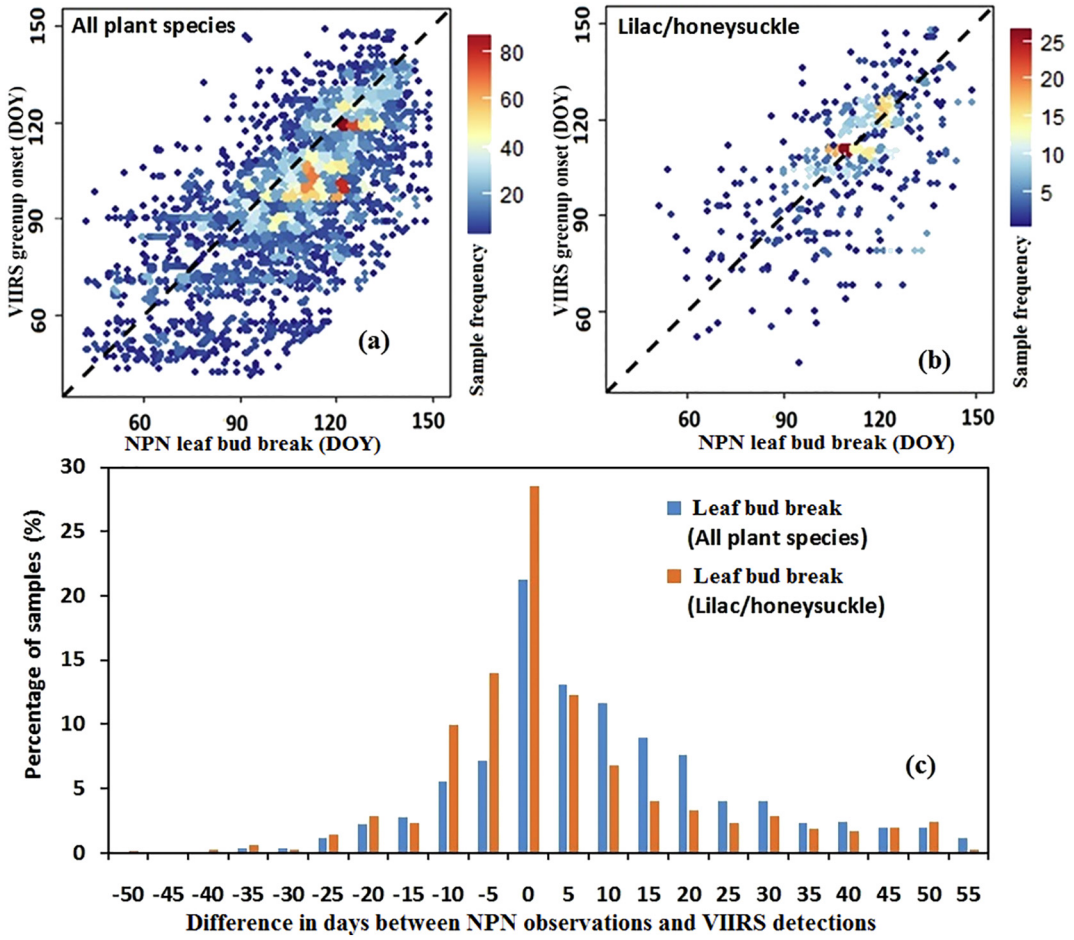

Fig. 8. Comparisons of the VIIRS LSP detections with the USA-NPN observations during 2013 and 2014: (a) regression for leaf bud break across all species ($y = -4.57 + 0.977x$, $R = 0.655$, $n = 5821$), (b) regression for leaf bud break in lilac and honeysuckle clones only ($y = 1.06 + 1.03x$, $R = 0.500$, $n = 705$), (c) the relative difference in days calculated as the USA-NPN observations minus the VIIRS detections. The dashed lines in panels (a) and (b) are the 1:1 lines.

dates from the VIIRS GLSP. As expected, the spatial pattern of these phenological dates differs across the CONUS. The pattern is spatially distinctive and very similar for the greenup and dormancy onsets, although the timing shifts along latitude in the eastern and central CONUS, where local gradients are interrupted by mountainous areas and by croplands. Over the western CONUS, however, the timing of greenup and dormancy onsets do not display such coherent spatial patterns. Similar to the greenup and dormancy onset, the mid-greenup and senescence dates also show geographic patterns, but are less distinct spatially. In contrast, the geographic patterns in both maturity and senescence onsets are very similar across central and eastern CONUS.

Latitudinal and longitudinal gradients in greenup are illustrated in Fig. 3. Timing of greenup onset depends strongly on latitude but the pattern is different in eastern and western regions (Fig. 3a). At 81.5°W, where forests dominate, greenup onset shows a clear gradient from DOY 60 in the south to DOY 150 in the north. It is interrupted by mountains (the Appalachian Mountains and the Allegheny Mountains located around 36°N–38°N), with a delay as large as one month, and by croplands (located around 42.8°N–44.3°N), with a delay as large as one and a half months relative to surrounding areas. In the central CONUS along the 91.0°W where croplands dominate, greenup onset is influenced by the timing of cultivation. Although a latitude gradient is evident, variation in greenup onset relative to neighboring pixels is distinctive because (1) natural vegetation tends to green up earlier than crops and (2) the timing of crop planting and subsequent greenup varies by crop types, e.g., corn (maize) is planted earlier than soybean. In the western region along at 108.5°W, greenup timing among neighboring pixels show high local variability, with differences as large as three months. Although the timing of greenup onset shows no latitudinal dependence from 35.5°N southwards, a distinct latitudinal gradient is identifiable from 37°N northwards. In contrast, longitudinal profiles show complex patterns (Fig. 3b) in which greenup shifts later from the west coast to the Rocky Mountains, shows a weak gradient that reflects changes in elevation on the eastern slope of the Rocky Mountains, and remains relatively stable with little variation as a function of longitude in the eastern region. All three profiles reveal that the timing of greenup display substantially variability from 100°W westwards, and that in the eastern CONUS, notable differences are observable between the southern (~30.5°N) and northern (45°N) regions.

4.3. Spatial patterns in LSP amplitude

Fig. 4 presents maps showing the EVI2 amplitude at each pixel, based on the EVI2 values on the greenup and maturity onset dates. Overall greenness displays a distinct spatial variation across the CONUS, in which EVI2 is low in the most western CONUS (except in the northwest), and high in eastern regions. However, the EVI2 value on the greenup onset date shows much more spatial variation than the corresponding values on the maturity date. EVI2 greenness at greenup onset is slightly lower in croplands relative to the surrounding natural vegetation, but is slightly higher in the southern region than in the northern region. In contrast, the EVI2 greenness at maturity onset is generally > 0.4 in the eastern region, with the highest EVI2 values in the central CONUS croplands and in the eastern deciduous forests.

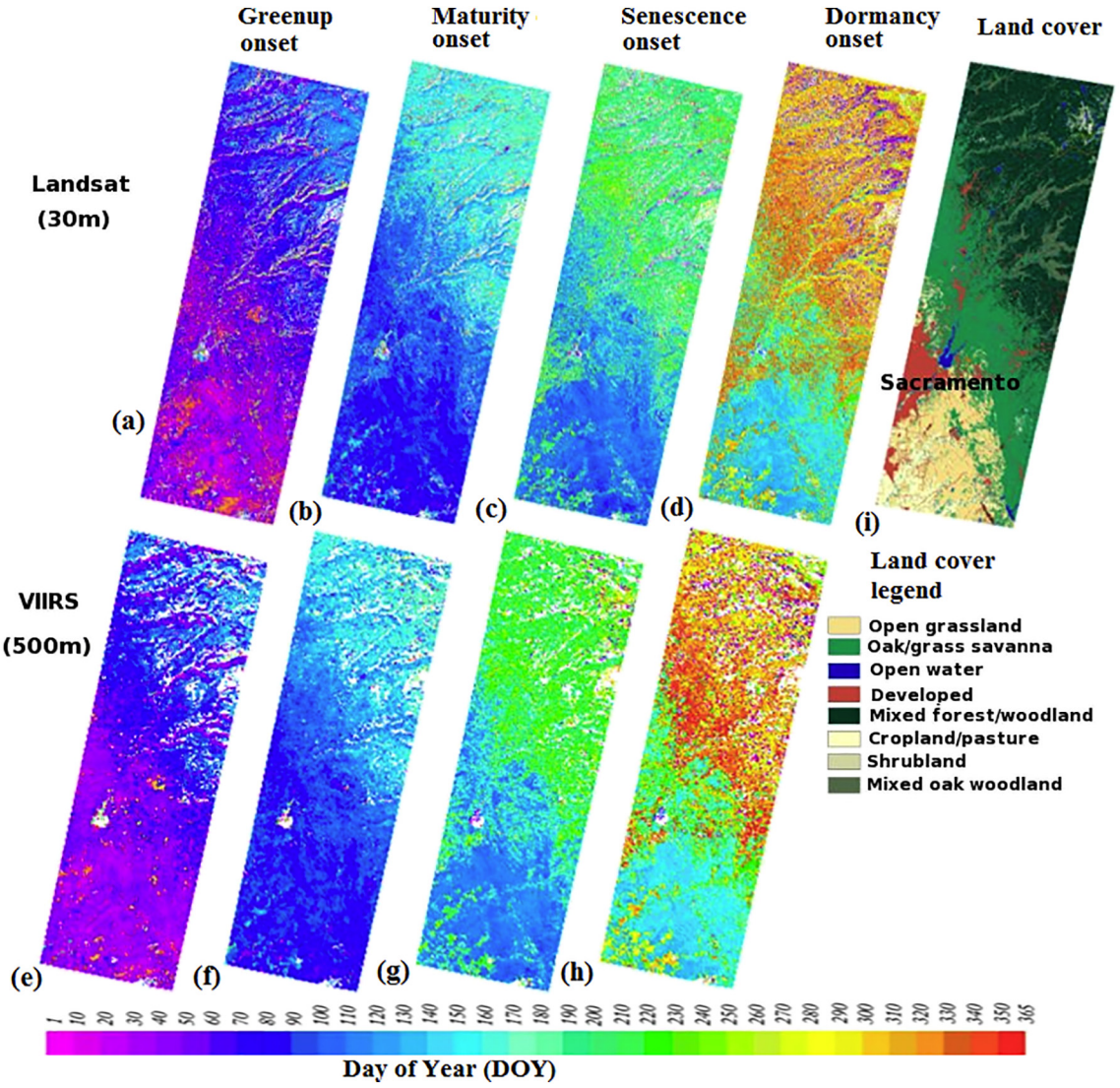

Fig. 9. Spatial pattern of the phenological timing detected from Landsat (a–d) and VIIRS time series (e–f) in the overlap zone between Landsat path 43/row 33 and path 44/row 33 in California in 2013. The four phenological transition dates are greenup onset (a and e), maturity onset (b and f), senescence onset (c and g), and dormancy onset (d and h). The land cover type is shown in (i).

Overall, unlike the phenological transition dates, the EVI2 greenness is more strongly dependent on land cover types than latitudinal or longitudinal gradients.

Profiles of EVI2 greenness as a function of latitude and longitude reflect variation in land cover types (Fig. 5). The profile along 81.5°W provides EVI2 greenness variations from the south to the north (Fig. 5a). From 34°N southwards, where land cover is complex (although mixed forests and woody savannas dominate), the EVI2 at greenup onset is quite high (ranging from 0.3–0.4) and the EVI2 at maturity onset varies primarily between 0.4 and 0.6, resulting in a relatively modest EVI2 amplitude during the growing season. In the region between 35°N–40°N, where deciduous forests dominate, the EVI2 at greenup onset is < 0.25, while the EVI2 at maturity onset is over 0.70, leading to the largest EVI2 amplitudes (~0.5). In the regions from 40°N–44°N, which are covered by croplands (including croplands and natural vegetation mosaics), the EVI2 amplitude is large, and only slightly smaller than those from deciduous forests. From 46°N northward, the evergreen and mixed forests display lower EVI2 values at maturity onset, with associated EVI2 amplitudes of ~0.2. Along longitude at 37°N (Fig. 5b), however, EVI2 values at both the greenup and maturity onset are relatively large, with considerable variation among neighboring pixels from 118°W westward, where the land cover includes a mosaic of evergreen forests, mixed forests, savannas, grasslands, and croplands. EVI2 values on both phenological dates in the region from 118°W to 81.4°W gradually increases, and the EVI2 amplitude increases accordingly. EVI2 values are very small in open shrublands and barren lands, and increase in grasslands, croplands (including croplands/natural vegetation mosaics), and in deciduous and mixed forests.

4.4. Assessment of the quality of VIIRS phenology detections

The quality of the VIIRS NBAR EVI2 data is illustrated using three tiles across the CONUS: tile h11v04 (central CONUS), h12v04 (northeastern CONUS), and h08v05 (western CONUS). Tile h11v04 includes 53% croplands and 22% cropland/natural vegetation mosaics; tile h12v04 contains 70% of deciduous and mixed forests; and tile h08v05 is comprised of land cover types including shrublands (56%), savannas (8%), grasslands (13%) and barren (9%).

In the central CONUS (tile h11v04), the AI between the HLPM modeled EVI2 and the high quality EVI2 observations during the growing season is > 80% (Figs. 6a and 7d), which indicates that the HLPM captures the temporal EVI2 trajectory effectively for individual pixels. The PHQ of the EVI2 observations during the vegetation growing

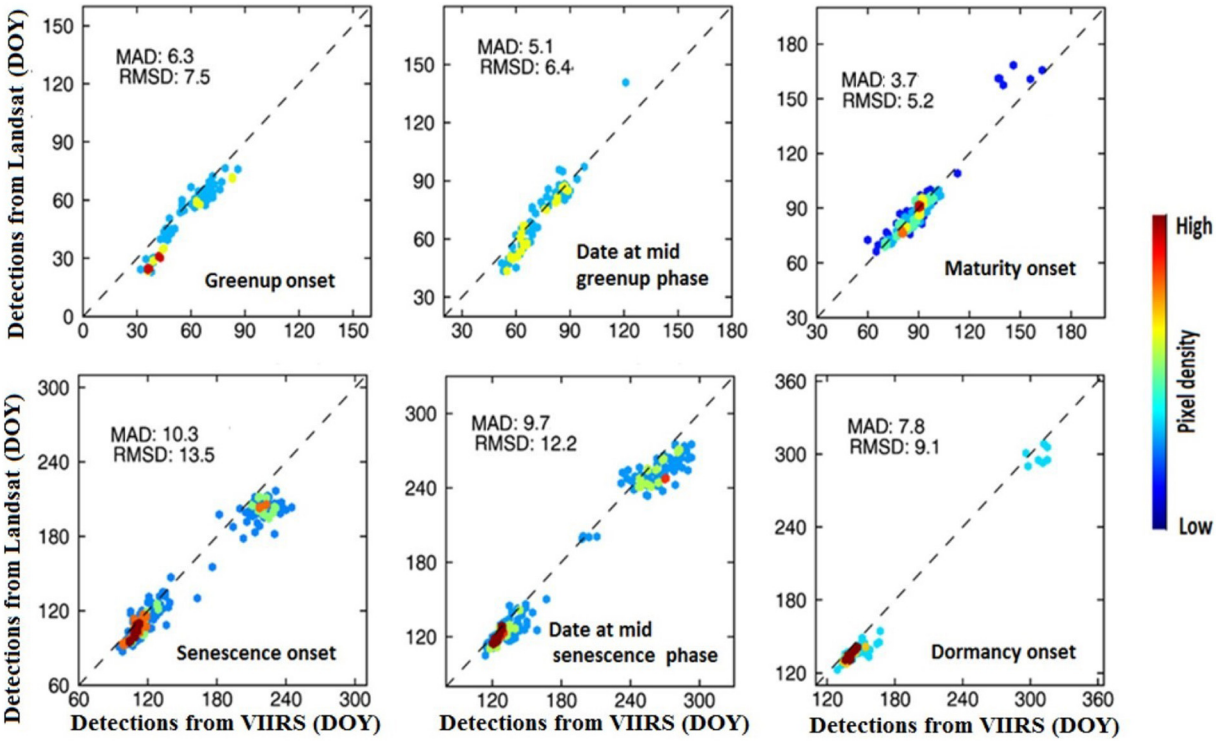

Fig. 10. Scatterplots of phenological transition dates detected from Landsat and VIIRS data in the path overlap zone between Landsat WRS-2 path 43/row 33 and path 44/row 33 in California. Note that the samples are from pixels with relatively homogeneous phenological dates that differ greatly between grasslands/savannas and forests. MAD is mean absolute difference and RMSD is root mean square difference.

Table 1
Mean absolute difference (in days) in the phenological dates between the VIIRS and Landsat detections in the overlapping zone between Landsat path 43/row 33 and path 44/row 33 in California in 2013.

Land cover	Greenup onset	Date at mid-greenup phase	Maturity onset	Senescence onset	Date at mid-senescence onset	Dormancy onset
Grasslands	7.6	6.4	4.4	8.9	9.7	10.3
Savannas	4.4	3.1	4.1	13.2	16.1	15.0
Mixed forests	8.3	7.1	7.5	17.3	15.6	13.8

season is > 60% for most pixels, although it is somewhat higher in western areas than in eastern regions (Figs. 6b and 7d). This indicates that the EVI2 time series is of overall high quality. However, the LPHQ of EVI2 observations around each phenological transition date is unique and differs greatly across the region (Fig. 6c–f). This implies that the time and duration of cloud contaminated observations exhibit high spatial variation during the growing season. For the four key phenological transition dates, the LPHQ is largest around the senescence onset, followed by maturity onset, greenup onset, and dormancy onset. Accordingly, the proportion of pixels with LPHQ > 60% is about 75% around senescence onset, 62% around maturity onset, 55% around greenup onset, and 50% around dormancy onset (Fig. 7a).

In tile h12v04 the LPHQ < 60% appears in about 75% of the land pixels at dormancy onset, and in about 50% of the pixels at greenup, maturity, and at senescence onsets (Fig. 7b). The PHQ during the growing season is also relatively poor, although the agreement index is high (Fig. 7d). In contrast, in the arid and semiarid environments of tile h08v05, the LPHQ is larger than 60% for each phenological transition date in > 90% of land pixels (Fig. 7c). However, the HPLM agreement index is relatively poor with AI < 80% in 25% of pixels because of the irregular EVI2 variations and the indistinguishable seasonality (Fig. 7d). In addition, interannual variation in the LPHQ between 2013 and 2014 (not shown) is substantial.

4.5. Evaluation of phenology detections in VIIRS GLSP

4.5.1. Comparison with field observations

Fig. 8 compares the VIIRS phenology detection dates with USA-NPN ground level phenological observations. The geometric mean functional regression indicates that VIIRS greenup onset date is very comparable with the timing of leaf bud break for both the USA-NPN observations and individually for the lilac and honeysuckle clone data. The slope is close to one, implying that the phenological timing from VIIRS GLSP reflect the field observations very well, both spatially and interannually. The negative intercept in the relationship for all plant species reveals that the VIIRS detections are biased 5 days early compared to the USA-NPN observed spring events. The intercept of one in the relationship for the lilac and honeysuckle clones indicates that VIIRS detections represent nearly identical timing of leaf bud break in these two species.

Further analysis indicates that the relative difference between the VIIRS detections and the USA-NPN observations for all plants and for just the lilac and honeysuckle clones is < 10 days and 15 days in 59% and 72% of samples, respectively, and < 15 days in 70% and 78% of samples, respectively (Fig. 8c).

4.5.2. Comparison with high resolution satellite detections

Fig. 9 presents the phenological timing detected from Landsat and VIIRS data in 2013 in the Sierra Nevada Mountains, California. Visual

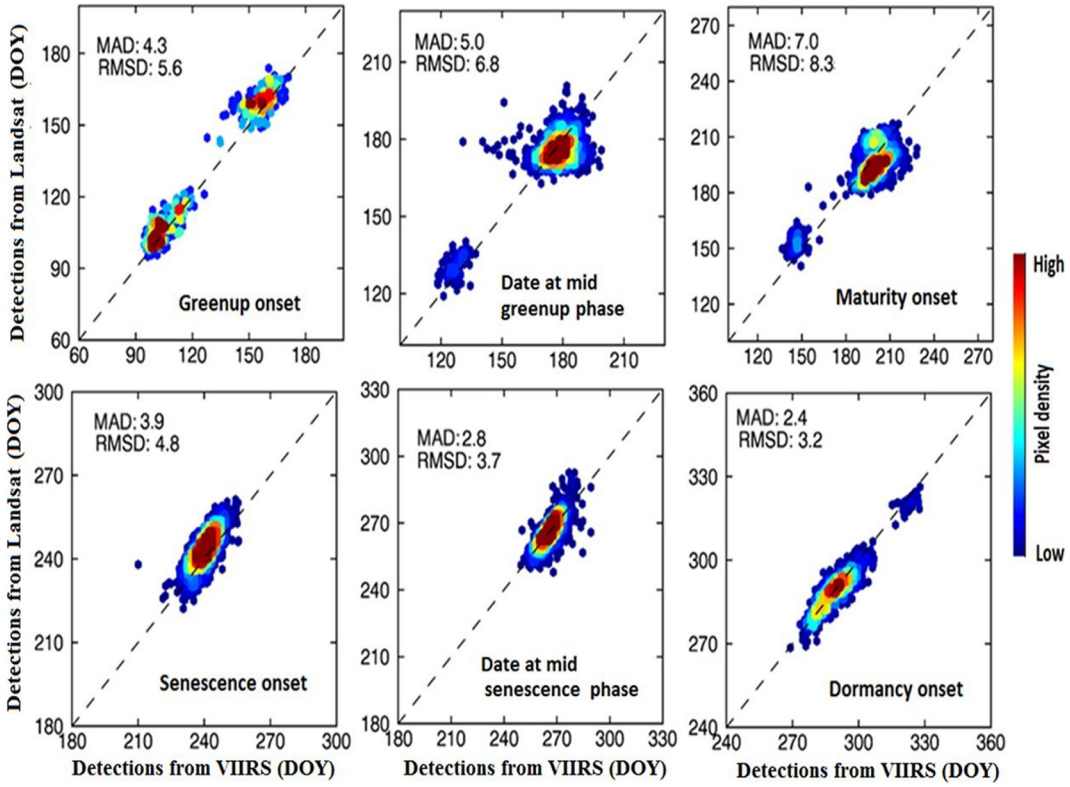

Fig. 11. Comparison of the six phenological dates detected from the VIIRS NBAR EVI2 (500 m) and the fused MODIS-Landsat OLI data (30 m) in 2013 for a location in the central US (Landsat WRS-2 path 26/row 31). Note that the samples are from pixels with relatively homogeneous phenological dates that differ greatly between croplands and forests. MAD is mean absolute difference and RMSD is root mean square difference.

inspection shows that the spatial patterns are similar between the Landsat and VIIRS detections for the four key phenological transition dates. The phenological timing for both datasets is earlier in the southern region, which is dominated by grasslands and savannas, and is later in the northern region, which is covered with mixed forests and woodlands.

An analysis, based on 20% of the most homogeneous pixels, indicates that the mean absolute difference (MAD) in phenological dates ranges from 4 to 6 days during the greenup phase (i.e. greenup onset, date at mid-greenup phase, and maturity onset) and from 8 to 10 days during the senescence phase (i.e. senescence onset, date at mid-senescence phase, and dormancy onset) (Fig. 10). The corresponding RMSE is 5–8 days and 9–14 days, respectively. All of the sample pairs are distributed along the 1:1 line, although the Landsat detections tend to be biased slightly later relative to the VIIRS detections. Comparison of phenological dates stratified by the dominant land cover types in this region indicates that the MAD is smaller in savannas during the greenup phase and smaller in grasslands during the senescence phase (Table 1).

Fig. 11 presents a comparison between phenological detections from VIIRS and those estimated from fused MODIS-Landsat OLI data (30 m) in 2013 in the central CONUS. In 20% of the most homogeneous pixels that are dominated by croplands (corn and soybean) and forests, the MAD between these two sets of land surface phenology detections is < 5 days for all transition dates except maturity onset, and the RMSD is < 8 days for all six phenological timing metrics. The samples are generally distributed along the 1:1 line without an obvious bias.

4.5.3. Comparison with MODIS phenology detections

The similarity between the VIIRS and the MODIS phenology detections is illustrated using the greenup onset (as it is the most important phenological metric in a vegetation growth cycle). Overall, the greenup onset dates from these two products are comparable and without bias, with median differences of < 1 day between the VIIRS and MODIS greenup onset. > 50% and 76% of pixels show greenup onset differences of < 5 days and 10 days, respectively, in tiles h11v04 and h12v04. The timing differences are somewhat larger in tile h08v05, which shows differences of < 5 days and 10 days in 44% and 66% of pixels, respectively.

After fine-scale heterogeneity caused by local heterogeneity and differences in the effective size of MODIS and VIIRS pixels were filtered by spatially smoothing the greenup onset dates using a 3 × 3 moving window, the similarity of the VIIRS detections to the MODIS detections greatly increases (Fig. 12). Specifically, after applying this filtering, greenup onset differences of < 5 days and < 10 days account for 68% and 91% of pixels across the tile h12v04, respectively. Relatively large differences are still evident in evergreen forests and shrublands, while small differences are found in mixed and deciduous forests. Patterns of differences in the greenup onset in tile h11v04 are similar to those in tile h12v04. However, the proportion of pixels in tile h11v04 for each land cover type is larger than 63% and 87% for differences of < 5 and < 10 days, respectively. In semiarid land cover types (tile h08v05), the difference between the VIIRS and MODIS phenology detections is somewhat larger. Over 58% and 78% of pixels exhibited differences of < 5 and < 10 days, respectively, with larger differences in the evergreen forests and savannas.

Fig. 13 shows the frequency of pixels stratified by the local proportion of high quality (LPHQ) observations around each phenological transition date from the MODIS and VIIRS NBAR EVI2 time series in 2013. Around the four key phenological dates, the proportion of pixels with a low LPHQ is generally higher in the VIIRS EVI2 time series than in the MODIS EVI2 time series, indicating that there are more pixels in the MODIS time series that have higher LPHQ relative to the VIIRS EVI2 time series, although this difference varies among phenological onset periods (events) and across regions. In tile h11v04, the LPHQ for the MODIS EVI2 time series is only slightly larger than that in the VIIRS time series. For example, the pixel proportion with a LPHQ > 80% is

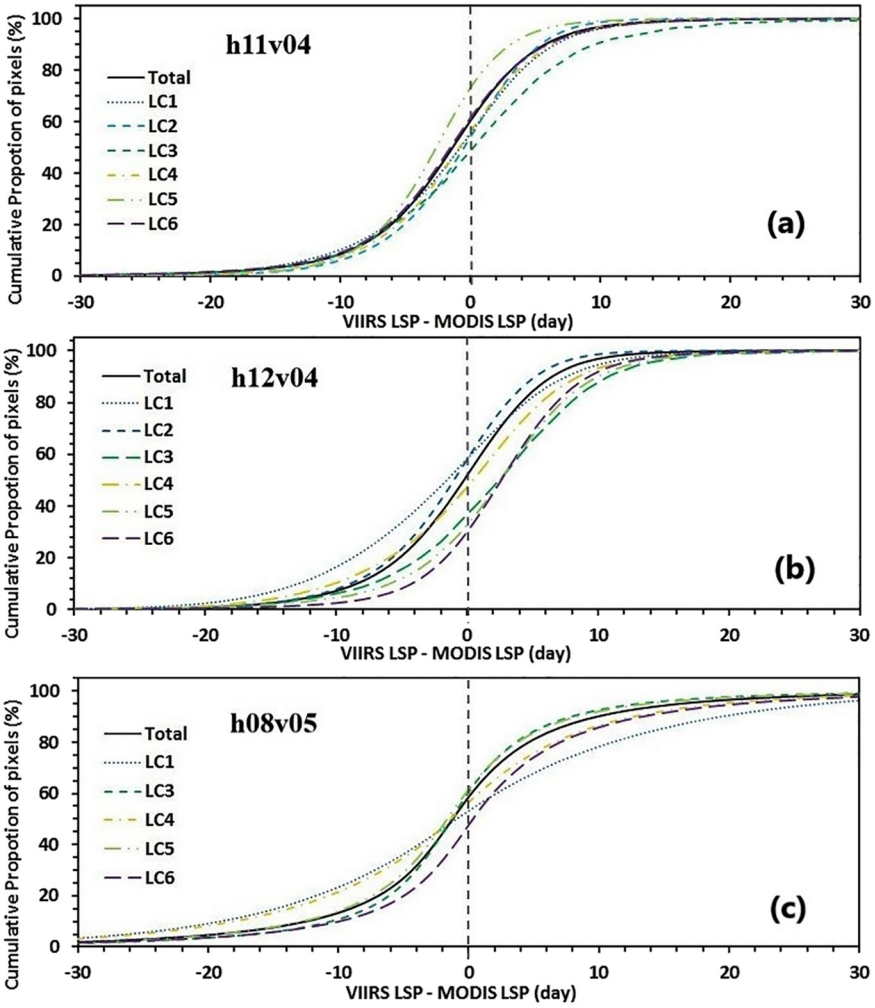

Fig. 12. Comparison of the greenup onset dates between the VIIRS and MODIS detections in 2013 for tiles (a) h11v04, (b) h12v04, and (c) h08v05. Total - all land cover types, LC1-evergreen forest, LC2-mixed forests and deciduous forests, LC3 – open shrublands and close shrublands, LC4 – savannas and woody savannas, LC5 – grasslands, LC6 – cropland and natural vegetation mosaic.

only 4%, 7%, 8%, and 7% larger in the MODIS than in the VIIRS data around the greenup, maturity, senescence, and dormancy onset dates, respectively (Fig. 13a). In tile h12v04, the proportion of pixels with LPHQ > 50% is 15%, 19%, 1%, and 8% higher in the MODIS NBAR time series than in the VIIRS NBAR data around the four key phenological dates, respectively, and the proportion with LPHQ > 80% is 34%, 20%, 5%, and 5% larger in the MODIS NBAR time series than in the VIIRS NBAR time series (Fig. 13b).

The quality of MODIS and VIIRS time series significantly impacts the discrepancy between MODIS and VIIRS GLSP detections. This can be illustrated by plotting the greenup onset differences as a function of LPHQ (Fig. 14). The cumulative proportion of pixels with small differences between the VIIRS and MODIS greenup onset dates is highest when LPHQ = 80–100, followed by LPHQ = 40–80, LPHQ = 10–40, and LPHQ = others. In tile h11v04, the proportion of pixels is 60%, 53%, 53%, and 38% for greenup onset differences less than five days for a LPHQ = 80–100, LPHQ = 40–80, LPHQ = 10–40, and LPHQ = others, respectively, and is 86%, 78%, 76%, and 63% for the differences less than ten days (Fig. 14a). In tile h12v04, the proportion of pixels is 60%, 43%, 42%, and 20% for differences less than five days for the LPHQ = 80–100, LPHQ = 40–80, LPHQ = 10–40 LPHQ = others, respectively, and 86%, 68%, 66%, and 36% for phenological differences less than ten days (Fig. 14b). Similar impacts are found for other phenological onsets dates (results are not shown here.) These results suggest that retrieved phenological dates are highly comparable between the MODIS and VIIRS detections if the quality of EVI2 time series from both datasets are similarly high, but that the differences can be quite large if their corresponding EVI2 quality values are low or very different.

5. Discussion

Implementation of the VIIRS GLSP algorithm across the CONUS demonstrates its ability to detect the phenological metrics across the seasonal pattern of vegetation growth. The resultant products reveal clear spatial patterns in phenological transition dates. VIIRS GLSP phenological transition dates show latitudinal gradients in the eastern and central CONUS, although these gradients are frequently interrupted by mountains and croplands. In contrast, the VIIRS GLSP phenological dates show no regular pattern as a function of latitude in the arid western CONUS. Along longitudinal transects, the phenological dates vary irregularly in the western CONUS, but remain relatively stable in the central and eastern CONUS. The overall spatial pattern of greenup onset over the CONUS is consistent with available phenology detections from AVHRR and MODIS (Ganguly et al., 2010; Julien and Sobrino, 2009; Tan et al., 2011; Zhang et al., 2014), but local differences can be substantial. Overall, our results demonstrate that the VIIRS GLSP product provides comprehensive and consistent phenological dates throughout a vegetation growing season, including the greenup onset, maturity onset, senescence onset, dormancy onset, and the dates at mid-

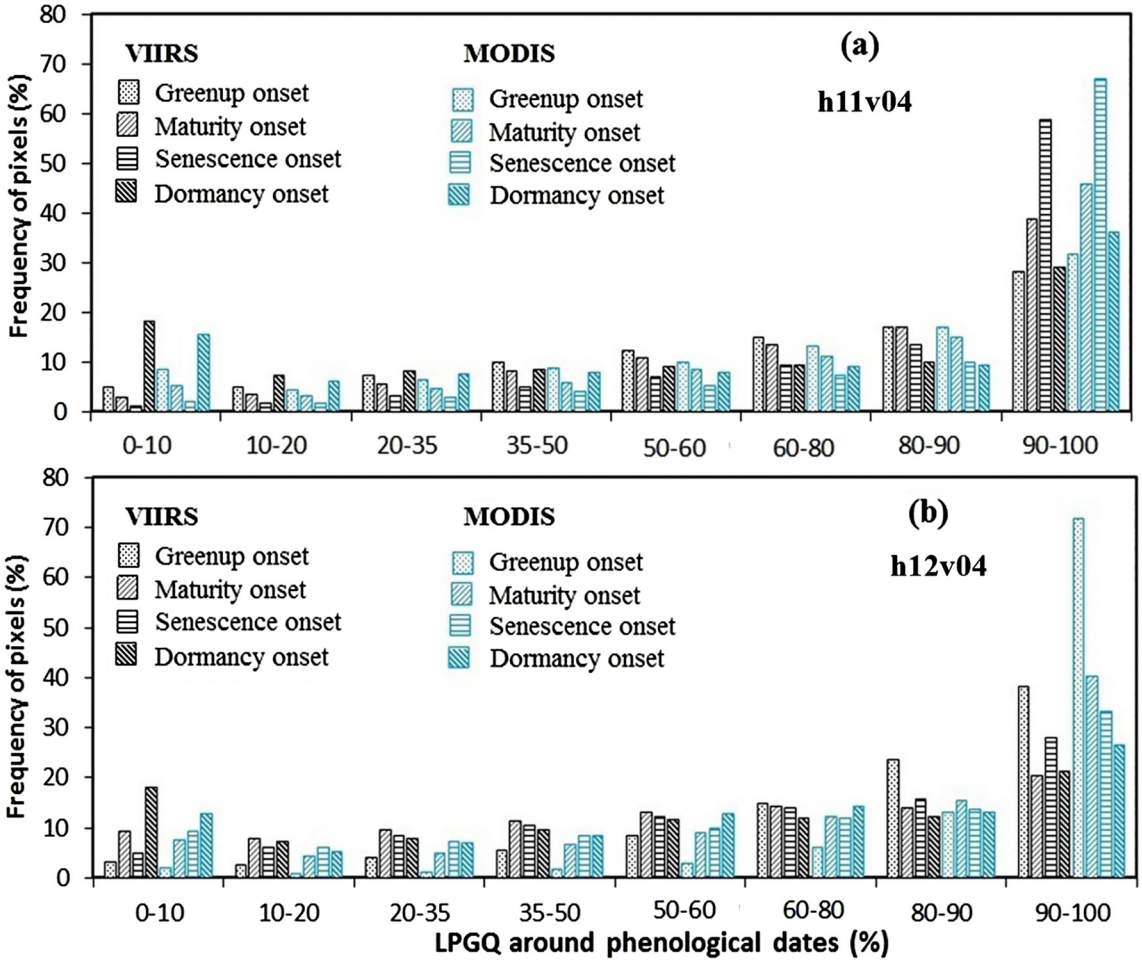

Fig. 13. Variation of pixel frequency against the local proportion of high quality (LPHQ) observations around the four key phenological transition dates between the MODIS and VIIRS NBAR EVI2 time series in 2013.

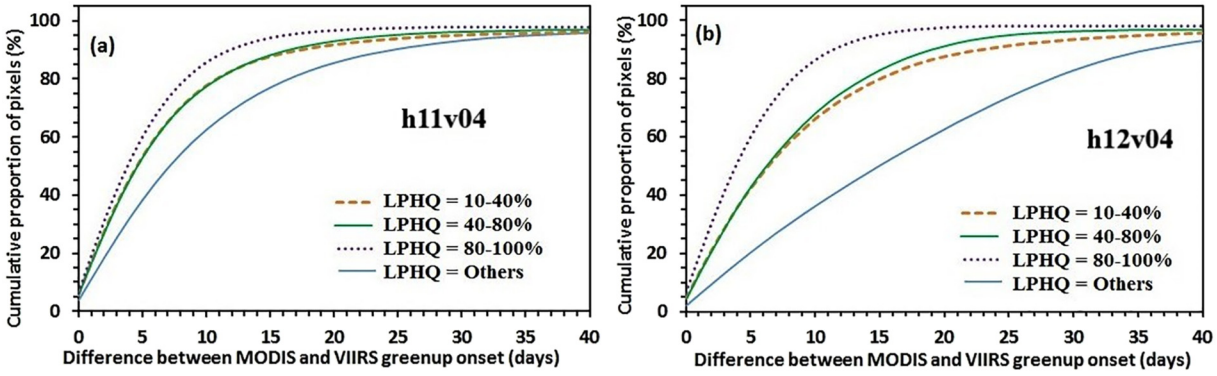

Fig. 14. Cumulative proportion of pixels varying with the absolute difference (days) between the VIIRS and MODIS greenup onset dates for four categories of local EVI2 quality (LPHQ) during 2013 in (a) tile h11v04 and (b) tile h12v04.

greenup and mid-senescence phases. The VIIRS GLSP product also characterizes the magnitude in phenological variation in vegetation greenness at greenup onset, maturity onset, and throughout the growing season. Note the latter is not presented here. Spatial patterns in greenness depend strongly on land cover type, where greenness amplitude is larger in deciduous forests, mixed forests, and croplands, and smaller in shrublands and grasslands.

In addition to the phenological dates and the greenness magnitude during the growing season, the VIIRS GLSP product also provides corresponding metrics of confidence and quality in the phenology detections. The confidence in phenology detections is controlled by the quality of time series provided by VIIRS. The VIIRS NBAR product provides reliable vegetation indices for cloud-free observations because the atmospheric and bidirectional effects have been corrected (Liu et al., 2017b). However, missing land surface observations caused by cloud cover introduce gaps in VIIRS NBAR time series. The overall data quality, quantified using the proportion of high quality observations and the agreement index between the HPLM and the high quality EVI2 observations during each growing season offers assessments of the quality of the time series for phenology detections. The agreement

index is particularly important for quantifying a measure of confidence in phenology detections in arid environments, where the cloud-contaminated observations are generally limited but temporal variation in EVI2 is subtle and somewhat irregular.

The frequency of missing observations around the timing of greenup, maturity, senescence, and dormancy onset is inconsistent across pixels and between years, although there is generally more cloud contamination in humid climates than in arid climates. Large amounts of missing observations generally lead to lower confidence in VIIRS GLSP detections, which is evident in results from the comparison between MODIS and VIIRS time series around greenup onset dates. Similar impacts of the time-dependent local data quality of the other phenological transition dates are also significant, although these details are not presented here. However, it should be noted that poor quality of EVI2 time series data will result in lower confidence in phenology detections, but do not necessarily lead to large errors.

Assessment of the VIIRS GLSP product quality based on reference data is important but is currently challenging: in situ observations that are both temporally and spatially matched with VIIRS footprints do not exist and are not likely to become available anytime soon. Here rely on extensive comparative evaluations, using a variety of independent data sources to improve our understanding of VIIRS GLSP quality. In a separate study (Zhang et al., 2018), the six phenological transition dates from VIIRS GLSP product have been compared with PhenoCam observations across the CONUS. Those results demonstrate that the mean absolute difference between the VIIRS EVI2 and PhenoCam phenological dates is 7–11 days in the greenup phase and 10–13 days in the senescence phase as based on 164 site-years during 2013 and 2014 across multiple land cover types. But, again, it is important to note that PhenoCam phenological dates provide a local estimate that does not reflect the spatial unit of measurement acquired by VIIRS.

The quality assessment evaluations presented in this study indicate that the VIIRS GLSP algorithm provides high quality representations of in-situ phenology. Comparison with species-specific observations from the USA-NPN suggests that the VIIRS greenup onset reflect the leaf bud break timing across plant species quite well, although with a systematic lag of 5 days. The mean absolute difference between the VIIRS greenup onset and the leaf bud break timing in all plant species was < 10 days for most VIIRS pixels. Comparison using only cloned lilacs and honeysuckles show even stronger agreement. It is well-known that species-specific leaf bud break timing is not exactly the same as satellite-based phenological detections because of the mismatch between individual species in ground observations and vegetation community sensed within a satellite pixel (Ganguly et al., 2010; Liang and Schwartz, 2009; Morisette et al., 2009; White et al., 2009; Zhang and Goldberg, 2011). However, phenological timing is primarily driven by local weather and the response of underlying vegetation types (Delbart et al., 2015; Mazer et al., 2015; Piao et al., 2007; Piao et al., 2015; Wu et al., 2014), which results in spatial continuity or gradual variation in phenological transition dates across regions with coexisting species presenting similar phenological dates. As a result, although species-specific observations and VIIRS detections are not necessarily comparable for each individual VIIRS pixel and their difference can be quite large, the large number of samples available from the USA-NPN observations across the CONUS that are used in this study exhibit consistent spatial and interannual covariation with VIIRS phenology detections.

The VIIRS GLSP results show good agreement with phenology detections from 30 m Landsat data. Our evaluation demonstrates that all six phenological transition dates in VIIRS GLSP are closely comparable to Landsat detections with an absolute difference < 10 days in relatively homogeneous VIIRS pixels, and the agreement in croplands, savannas, and forests is similar. Although both the VIIRS and Landsat phenological dates are derived from the same vegetation index, the 30 m pixel footprint of Landsat data is better able to monitor phenology for small areas with homogeneous vegetation types, thus offering a more realistic dataset for assessing error and uncertainty in the VIIRS GLSP product (Klosterman et al., 2014; Kovalskyy et al., 2012). In addition, Landsat-derived phenology has an advantage over ground based measurements for spatiotemporally matching with the VIIRS GLSP pixel footprint and providing more reliable comparative evaluations.

Comparison of VIIRS GLSP results with MODIS GLSP results allow us to understand differences and similarities between these two products. This comparison is critical to establish a long-term environmental data record of land surface phenology with the VIIRS GLSP that extends the established record from MODIS. Comparison of phenological transition dates in mixed and deciduous forests, croplands, and semiarid savannas and shrublands revealed that GLSP detections from MODIS and VIIRS are similar, without bias, and that their difference in most pixels is < 10 days (although this discrepancy is larger in semiarid savannas and shrublands). Differences between MODIS and VIIRS GLSP arises from several sources. First, vegetation indices produced from MODIS and VIIRS are not necessarily consistent (Vargas et al., 2013), and the biases between the MODIS and VIIRS EVI2 time series can be inconsistent in both space and time (Zhang et al., 2017b). Second, there are more cloud-free retrievals in MODIS NBAR EVI2 time series than in the VIIRS NBAR EVI2 time series because the MODIS NBAR product uses observations from the MODIS instrument on both Terra and Aqua (Wang et al., 2012), whereas, the VIIRS NBAR product is generated from only the VIIRS onboard Suomi NPP (i.e., from a single, early afternoon overpass) (Liu et al., 2017b). Third, although the nominal gridded spatial resolution of both the MODIS and VIIRS NBAR products is 500 m, the effective pixel footprint (area) is 1.34 times of the 500 m grid area for the VIIRS data and 2.06 times of that for the MODIS data (Campagnolo et al., 2016). As a result, inconsistencies between VIIRS GLSP and MODIS GLSP products do exist. Post-processing of MODIS and VIIRS GLSP products, with a 3 × 3 moving windows to spatially smooth the data, can significantly mitigate this difference, although this then reduces the spatial details to some degree.

Finally, VIIRS GLSP is characterized using time series of EVI2 while various other phenology products from other sensors have been derived from NDVI. Therefore, comparisons between EVI2 and NDVI phenology retrievals might provide some further context in utilizing VIIRS GLSP. However, no direct comparison is performed in this paper, as a variety of previous studies have already demonstrated the advantages of EVI2 time series for phenology detections over NDVI data. Specifically, comparison of phenological metrics between VIIRS EVI2 and NDVI detections in 164 sites-year during 2013–2014 across the CONUS has shown that their mean absolute difference (MAD) is < 6 days in spring phenophase transition dates while it is 10.5–18.4 days in autumn senescence phenophase transition dates (Zhang et al., 2018). Compared with the PhenoCam phenology as a proxy for ground observations, it has been further demonstrated that the uncertainty (MAD) is 6.9–11.0 days for VIIRS EVI2 detections and 7.3–11.1 days for VIIRS NDVI detections in spring phenophase transition dates while it is 10.0–13.0 days for VIIRS EVI2 detections and 16.1–23.3 days for VIIRS NDVI detections in autumn phenophase transition dates (Zhang et al., 2018). This result reveals that EVI2 data could provide better phenology detections than NDVI, particularly during senescence phases. This pattern is also supported by the phenological metrics derived from Landsat and MODIS time series. Relative to field measurements, the uncertainty in greenup onset is 11 days from Landsat EVI and 18 days from Landsat NDVI (White et al., 2014). Further, MODIS EVI phenology is relatively better than MODIS NDVI phenology when compared with PhenoCam phenological dates for deciduous forests in the northwestern CONUS (Klosterman et al., 2014), with ground observed phenology from both USA-NPN and AmeriFlux observations across the CONUS (Peng et al., 2017a), and 81 site-year flux tower observations in the Northern Hemisphere boreal zone (Karkauskaite et al., 2017). These differences are mainly associated with the following factors: (1) NDVI is sensitive to background reflectance (soil background brightness and moisture condition) (Bausch, 1993; Huete et al., 1985) and the saturation at densely vegetated areas (Gitelson, 2004; Huete et al., 2002;

Vina et al., 2004); however, EVI2 (or EVI) reduces sensitivity to soil and atmospheric effects, and remains sensitive to variation in canopy density where NDVI becomes saturated (Huete et al., 2006; Rocha and Shaver, 2009). (2) NDVI and EVI2 characterize different biophysical properties of vegetation. Indeed, the EVI2 is more sensitive to vegetation gross primary production (GPP), net primary production (NPP), and FPAR (the fraction of photosynthetically active radiation) absorbed by chlorophyll ($FPAR_{chl}$); whereas, the NDVI is more representative of the total leaf variation on a vegetation canopy (including leaves with and without photosynthetic activities) and the FPAR absorbed by the canopy ($FPAR_{canopy}$) (Huete et al., 2013; Q.Y. Zhang et al., 2009; Zhang et al., 2005).

6. Conclusions

This paper provides an overview of the algorithm that is being used to generate the VIIRS global land surface phenology product, and presents preliminary results produced for the CONUS. The HPLM used for the VIIRS GLSP product models vegetation greenness phenology using biophysically meaningful parameters, allows for both symmetric and asymmetric EVI2 greenness development (Elmore et al., 2012; Melaas et al., 2013), and identifies key phenological transition dates using the change rate of greenness curvature instead of predefined thresholds. Thus, the VIIRS GLSP algorithm is able to detect phenological dates across a range of vegetation types and climate regimes.

Results from the comprehensive evaluation of the VIIRS GLSP across the CONUS demonstrates that the product provides high quality results and should meet the needs of the scientific community for characterizing large scale phenological dynamics and change. The VIIRS GLSP product will be produced operationally and globally by NASA from 2012 forward on a yearly basis starting in late 2018. It is a level 3 product and follows the structure and file format in the high level of global VIIRS data. The details of the phenological metric layers and data format are described in the VIIRS GLSP user guide (Zhang et al., 2017a). Note that more extensive and comprehensive evaluations will be conducted outside of the CONUS as these data become available, using multiple years of data to assure a continuous high quality GLSP data record. These efforts will include evaluations of VIIRS GLSP results using field observations and PhenoCam data in Europe and Asia, and using phenology data in diverse ecoregions using the NASA Harmonized Landsat-Sentinel-2 (HLS) data (https://hls.gsfc.nasa.gov/), which is producing a consistent, harmonized surface reflectance product from Landsat-8 OLI (Operational Land Imager) and Sentinel-2 MSI (MultiSpectral Instrument) data (Claverie et al., 2016). Finally, the VIIRS GLSP will also be improved by the incorporation of VIIRS observations from the JPSS1 platform, which was launched on November 18, 2017 (Goldberg et al., 2013).

Acknowledgements

This research was funded by NASA grant numbers NNX15AB96A and NNX14AQ18A. The authors thanks Jake Weltzin and Theresa Crimmins for providing field phenology observations from the United States of America National Phenology Network.

References

Allstadt, A.J., Vavrus, S.J., Heglund, P.J., Pidgeon, A.M., Thogmartin, W.E., Radeloff, V.C., 2015. Spring plant phenology and false springs in the conterminous US during the 21st century. Environ. Res. Lett. 10.

Ault, T.R., Henebry, G.M., de Beurs, K.M., Schwartz, M.D., Betancourt, J.L., Moore, D., 2013. The false spring of 2012, earliest in North American record. EOS Trans. Am. Geophys. Union 94, 181–182.

Ault, T.R., Schwartz, M.D., Zurita-Milla, R., Weltzin, J.F., Betancourt, J.L., 2015. Trends and natural variability of spring onset in the coterminous United States as evaluated by a new gridded dataset of spring indices. J. Clim. 28, 8363–8378.

Baldocchi, D., Falge, E., Wilson, K., 2001. A spectral analysis of biosphere-atmosphere trace gas flux densities and meteorological variables across hour to multi-year time scales. Agric. For. Meteorol. 107, 1–27.

Bausch, W.C., 1993. Soil background effects on reflectance-based crop coefficients for corn. Remote Sens. Environ. 46, 213–222.

Bradley, B.A., Jacob, R.W., Hermance, J.F., Mustard, J.F., 2007. A curve fitting procedure to derive inter-annual phenologies from time series of noisy satellite NDVI data. Remote Sens. Environ. 106, 137–145.

Campagnolo, M.L., Sun, Q.S., Liu, Y., Schaaf, C., Wang, Z.S., Roman, M.O., 2016. Estimating the effective spatial resolution of the operational BRDF, albedo, and nadir reflectance products from MODIS and VIIRS. Remote Sens. Environ. 175, 52–64.

Campbell, J.L., Rustad, L.E., Boyer, E.W., Christopher, S.F., Driscoll, C.T., Fernandez, I.J., Groffman, P.M., Houle, D., Kiekbusch, J., Magill, A.H., Mitchell, M.J., Ollinger, S.V., 2009. Consequences of climate change for biogeochemical cycling in forests of northeastern North America. Can. J. For. Res. 39, 264–284.

Chen, F., Dudhia, J., 2001. Coupling an advanced land surface-hydrology model with the Penn State-NCAR MM5 modeling system. Part I: model implementation and sensitivity. Mon. Weather Rev. 129, 569–585.

Chen, J., Jonsson, P., Tamura, M., Gu, Z.H., Matsushita, B., Eklundh, L., 2004. A simple method for reconstructing a high-quality NDVI time-series data set based on the Savitzky-Golay filter. Remote Sens. Environ. 91, 332–344.

Churkina, G., Schimel, D., Braswell, B.H., Xiao, X.M., 2005. Spatial analysis of growing season length control over net ecosystem exchange. Glob. Chang. Biol. 11, 1777–1787.

Claverie, M., Masek, J., Ju, J., 2016. Harmonized Landsat-8 Sentinel-2 (HLS) product user's guide. https://hls.gsfc.nasa.gov/wp-content/uploads/2017/02/HLS.v1.2.UserGuide.pdf.

Cleland, E.E., Chuine, I., Menzel, A., Mooney, H.A., Schwartz, M.D., 2007. Shifting plant phenology in response to global change. Trends Ecol. Evol. 22, 357–365.

Cleland, E.E., Allen, J.M., Crimmins, T.M., Dunne, J.A., Pau, S., Travers, S.E., Zavaleta, E.S., Wolkovich, E.M., 2012. Phenological tracking enables positive species responses to climate change. Ecology 93, 1765–1771.

Cooke, J.E.K., Weih, M., 2005. Nitrogen storage and seasonal nitrogen cycling in Populus: bridging molecular physiology and ecophysiology. New Phytol. 167, 19–30.

de Beurs, K.M., Henebry, G.M., 2004. Land surface phenology, climatic variation, and institutional change: analyzing agricultural land cover change in Kazakhstan. Remote Sens. Environ. 89, 497–509.

de Beurs, K.M., Henebry, G.M., 2005. Land surface phenology and temperature variation in the International Geosphere-Biosphere Program high-latitude transects. Glob. Chang. Biol. 11, 779–790.

de Beurs, K.M., Henebry, G.M., 2010. Spatio-temporal statistical methods for modeling land surface phenology. In: Hudson, I.L., Keatley, M.R. (Eds.), Phenological Research - Methods for Environmental and Climate Change Analysis. Spring, New York, pp. 177–208.

Delbart, N., Beaubien, E., Kergoat, L., Toan, T.L., 2015. Comparing land surface phenology with leafing and flowering observations from the PlantWatch citizen network. Remote Sens. Environ. 160, 273–280.

Denny, E.G., Gerst, K.L., Miller-Rushing, A.J., Tierney, G.L., Crimmins, T.M., Enquist, C.A.F., Guertin, P., Rosemartin, A.H., Schwartz, M.D., Thomas, K.A., Weltzin, J.F., 2014. Standardized phenology monitoring methods to track plant and animal activity for science and resource management applications. Int. J. Biometeorol. 58, 591–601.

Elmore, A.J., Guinn, S.M., Minsley, B.J., Richardson, A.D., 2012. Landscape controls on the timing of spring, autumn, and growing season length in mid-Atlantic forests. Glob. Chang. Biol. 18, 656–674.

EPA, 2016. Climate Change Indicators in the United States, Fourth Edition. . https://www.epa.gov/climate-indicators#explore.

Friedl, M., Henebry, G.M., Reed, B., Huete, A., White, M., Morisette, J., Nemani, R., Zhang, X., Myneni, R., 2006. Land Surface Phenology. A Community White Paperrequested by NASA. ftp://zeus.geog.umd.edu/Land_ESDR/Phenology_Friedl_whitepaper.pdf.

Ganguly, S., Friedl, M.A., Tan, B., Zhang, X.Y., Verma, M., 2010. Land surface phenology from MODIS: characterization of the Collection 5 global land cover dynamics product. Remote Sens. Environ. 114, 1805–1816.

Gao, F., Masek, J., Schwaller, M., Hall, F., 2006. On the blending of the Landsat and MODIS surface reflectance: predicting daily Landsat surface reflectance. IEEE Trans. Geosci. Remote Sens. 44, 2207–2218.

Gao, F., Anderson, M.C., Zhang, X., Yang, Z., Alfieri, J.G., Kustas, W.P., Mueller, R., Johnson, D.M., Prueger, J.H., 2017. Toward mapping crop progress at field scales through fusion of Landsat and MODIS imagery. Remote Sens. Environ. 188, 9–25.

Gerst, K.L., Kellermann, J.L., Enquist, C.A.F., Rosemartin, A.H., Denny, E.G., 2016. Estimating the onset of spring from a complex phenology database: trade-offs across geographic scales. Int. J. Biometeorol. 60, 391–400.

Gerten, D., Schaphoff, S., Haberlandt, U., Lucht, W., Sitch, S., 2004. Terrestrial vegetation and water balance - hydrological evaluation of a dynamic global vegetation model. J. Hydrol. 286, 249–270.

Gitelson, A.A., 2004. Wide dynamic range vegetation index for remote quantification of biophysical characteristics of vegetation. J. Plant Physiol. 161, 165–173.

Goldberg, M.D., Kilcoyne, H., Cikanek, H., Mehta, A., 2013. Joint Polar Satellite System: the United States next generation civilian polar-orbiting environmental satellite system. J. Geophys. Res.-Atmos. 118, 13463–13475.

Gray, J.M., Frolking, S., Kort, E.A., Ray, D.K., Kucharik, C.J., Ramankutty, N., Friedl, M.A., 2014. Direct human influence on atmospheric CO_2 seasonality from increased cropland productivity. Nature 515, 398 (+).

Heimann, M., Esser, G., Haxeltine, A., Kaduk, J., Kicklighter, D.W., Knorr, W., Kohlmaier, G.H., McGuire, A.D., Melillo, J., Moore, B., Otto, R.D., Prentice, I.C., Sauf, W., Schloss, A., Sitch, S., Wittenberg, U., Wurth, G., 1998. Evaluation of terrestrial carbon cycle models through simulations of the seasonal cycle of atmospheric CO_2: first results of a model intercomparison study. Glob. Biogeochem. Cycles 12, 1–24.

Henebry, G.M., de Beurs, K.M., 2013. Remote sensing of land surface phenology: a prospectus. In: Schwartz, M.D. (Ed.), Phenology: An Integrative Environmental Science. Springer, pp. 385–411.
Hogg, E.H., Price, D.T., Black, T.A., 2000. Postulated feedbacks of deciduous forest phenology on seasonal climate patterns in the western Canadian interior. J. Clim. 13, 4229–4243.
Huete, A.R., Jackson, R.D., Post, D.F., 1985. Spectral response of a plant canopy with different soil backgrounds. Remote Sens. Environ. 17, 37–53.
Huete, A., Didan, K., Miura, T., Rodriguez, E.P., Gao, X., Ferreira, L.G., 2002. Overview of the radiometric and biophysical performance of the MODIS vegetation indices. Remote Sens. Environ. 83, 195–213.
Huete, A.R., Didan, K., Shimabukuro, Y.E., Ratana, P., Saleska, S.R., Hutyra, L.R., Yang, W.Z., Nemani, R.R., Myneni, R., 2006. Amazon rainforests green-up with sunlight in dry season. Geophys. Res. Lett. 33.
Huete, A., Miura, T., Yoshioka, H., Ratana, P., Broich, M., 2013. Indices of vegetation activity. In: Hanes, J.M. (Ed.), Biophysical Applications of Satellite Remote Sensing. Spring, New York, pp. 1–41.
IPCC, 2007. Contribution of working group II to the fourth assessment report of the Intergovernmental Panel on Climate Change. In: Parry, M.L. (Ed.), Climate Change 2007: Impacts, Adaptation, and Vulnerability. Cambridge Univ. Press, Cambridge, pp. 976.
IPCC, 2014. In: Pachauri, R.K., Meyer, L.A. (Eds.), Climate Change 2014: Synthesis Report. Contribution of Working Groups I, II and III to the Fifth Assessment Report of the Intergovernmental Panel on Climate Change. Geneva, Switzerland, pp. 151.
Ivits, E., Cherlet, M., Toth, G., Sommer, S., Mehl, W., Vogt, J., Micale, F., 2012. Combining satellite derived phenology with climate data for climate change impact assessment. Glob. Planet. Chang. 88-89, 85–97.
Jakubauskas, M.E., Legates, D.R., Kastens, J.H., 2001. Harmonic analysis of time-series AVHRR NDVI data. Photogramm. Eng. Remote. Sens. 67, 461–470.
Jeong, S.J., Medvigy, D., Shevliakova, E., Malyshev, S., 2013. Predicting changes in temperate forest budburst using continental-scale observations and models. Geophys. Res. Lett. 40, 359–364.
Jiang, Z.Y., Huete, A.R., Didan, K., Miura, T., 2008. Development of a two-band enhanced vegetation index without a blue band. Remote Sens. Environ. 112, 3833–3845.
Jonsson, P., Eklundh, L., 2002. Seasonality extraction by function fitting to time-series of satellite sensor data. IEEE Trans. Geosci. Remote Sens. 40, 1824–1832.
Julien, Y., Sobrino, J.A., 2009. Global land surface phenology trends from GIMMS database. Int. J. Remote Sens. 30, 3495–3513.
Justice, C.O., Roman, M.O., Csiszar, I., Vermote, E.F., Wolfe, R.E., Hook, S.J., Friedl, M., Wang, Z.S., Schaaf, C.B., Miura, T., Tschudi, M., Riggs, G., Hall, D.K., Lyapustin, A.I., Devadiga, S., Davidson, C., Masuoka, E.J., 2013. Land and cryosphere products from Suomi NPP VIIRS: overview and status. J. Geophys. Res.-Atmos. 118, 9753–9765.
Karkauskaite, P., Tagesson, T., Fensholt, R., 2017. Evaluation of the plant phenology index (PPI), NDVI and EVI for start-of-season trend analysis of the northern hemisphere boreal zone. Remote Sens. 9.
Klosterman, S.T., Hufkens, K., Gray, J.M., Melaas, E., Sonnentag, O., Lavine, I., Mitchell, L., Norman, R., Friedl, M.A., Richardson, A.D., 2014. Evaluating remote sensing of deciduous forest phenology at multiple spatial scales using PhenoCam imagery. Biogeosciences 11, 4305–4320.
Korner, C., Basler, D., 2010. Phenology under global warming. Science 327, 1461–1462.
Kovalskyy, V., Roy, D.P., Zhang, X., Ju, J.C., 2012. The suitability of multi-temporal web-enabled Landsat data NDVI for phenological monitoring - a comparison with flux tower and MODIS NDVI. Remote Sens. Lett. 3, 325–334.
Liang, L., Schwartz, M., 2009. Landscape phenology: an integrative approach to seasonal vegetation dynamics. Landsc. Ecol. 24, 465–472.
Liu, Y., Hill, M.J., Zhang, X., Wang, Z., Richardson, A.D., Hufkens, K., Filippa, G., Baldocchi, D.D., Ma, S., Verfaillie, J., Schaaf, C.B., 2017a. Using data from Landsat, MODIS, VIIRS and PhenoCams to monitor the phenology of California oak/grass savanna and open grassland across spatial scales. Agric. For. Meteorol. 237–238, 311–325.
Liu, Y., Wang, Z., Sun, Q., Erb, A.M., Li, Z., Schaaf, C.B., Zhang, X., Roman, M.O., Scott, R.L., Zhang, Q., Novick, K.A., Bret-Harte, M.S., Petroy, S., SanClements, M., 2017b. Evaluation of the VIIRS BRDF, Albedo and NBAR products suite and an assessment of continuity with the long term MODIS record. Remote Sens. Environ. 201, 256–274.
Liu, Y., Wang, Z., Sun, Q., Erb, A.M., Li, Z., Schaaf, C.B., Zhang, X., Román, M.O., Scott, R.L., Zhang, Q., Novick, K.A., Bret-Harte, S., Petroy, S., SanClements, M., 2017c. Evaluation of the VIIRS BRDF, albedo and NBAR products suite and an assessment of continuity with the long term MODIS record. Remote Sens. Environ. 201, 256–274.
Mazer, S.J., Gerst, K.L., Matthews, E.R., Evenden, A., 2015. Species-specific phenological responses to winter temperature and precipitation in a water-limited ecosystem. Ecosphere 6.
Melaas, E.K., Friedl, M.A., Zhu, Z., 2013. Detecting interannual variation in deciduous broadleaf forest phenology using Landsat TM/ETM plus data. Remote Sens. Environ. 132, 176–185.
Melaas, E.K., Friedl, M.A., Richardson, A.D., 2016. Multiscale modeling of spring phenology across Deciduous Forests in the Eastern United States. Glob. Chang. Biol. 22, 792–805.
Moody, A., Johnson, D.M., 2001. Land-surface phenologies from AVHRR using the discrete fourier transform. Remote Sens. Environ. 75, 305–323.
Moore, K.E., Fitzjarrald, D.R., Sakai, R.K., Goulden, M.L., Munger, J.W., Wofsy, S.C., 1996. Seasonal variation in radiative and turbulent exchange at a deciduous forest in central Massachusetts. J. Appl. Meteorol. 35, 122–134.
Morisette, J.T., Richardson, A.D., Knapp, A.K., Fisher, J.I., Graham, E.A., Abatzoglou, J., Wilson, B.E., Breshears, D.D., Henebry, G.M., Hanes, J.M., Liang, L., 2009. Tracking the rhythm of the seasons in the face of global change: phenological research in the 21st century. Front. Ecol. Environ. 7, 253–260.
Moulin, S., Kergoat, L., Viovy, N., Dedieu, G., 1997. Global-scale assessment of vegetation phenology using NOAA/AVHRR satellite measurements. J. Clim. 10, 1154–1170.
Ollinger, S.V., Richardson, A.D., Martin, M.E., Hollinger, D.Y., Frolking, S.E., Reich, P.B., Plourde, L.C., Katul, G.G., Munger, J.W., Oren, R., Smithb, M.L., U, K.T.P., Bolstad, P.V., Cook, B.D., Day, M.C., Martin, T.A., Monson, R.K., Schmid, H.P., 2008. Canopy nitrogen, carbon assimilation, and albedo in temperate and boreal forests: functional relations and potential climate feedbacks. Proc. Natl. Acad. Sci. U. S. A. 105, 19336–19341.
Parmesan, C., Yohe, G., 2003. A globally coherent fingerprint of climate change impacts across natural systems. Nature 421, 37–42.
Peng, D., Wu, C., Li, C., Zhang, X., Liu, Z., Ye, H., Luo, S., Liu, X., Hu, Y., Fang, B., 2017a. Spring green-up phenology products derived from MODIS NDVI and EVI: Intercomparison, interpretation and validation using National Phenology Network and AmeriFlux observations. Ecol. Indic. 77, 323–336.
Peng, D.L., Zhang, X.Y., Wu, C.Y., Huang, W.J., Gonsamo, A., Huete, A.R., Didan, K., Tan, B., Liu, X.J., Zhang, B., 2017b. Intercomparison and evaluation of spring phenology products using National Phenology Network and AmeriFlux observations in the contiguous United States. Agric. For. Meteorol. 242, 33–46.
Piao, S.L., Friedlingstein, P., Ciais, P., Viovy, N., Demarty, J., 2007. Growing season extension and its impact on terrestrial carbon cycle in the Northern Hemisphere over the past 2 decades. Glob. Biogeochem. Cycles 21.
Piao, S.L., Tan, J.G., Chen, A.P., Fu, Y.H., Ciais, P., Liu, Q., Janssens, I.A., Vicca, S., Zeng, Z.Z., Jeong, S.J., Li, Y., Myneni, R.B., Peng, S.S., Shen, M.G., Pennuelas, J., 2015. Leaf onset in the northern hemisphere triggered by daytime temperature. Nat. Commun. 6.
Puma, M.J., Koster, R.D., Cook, B.I., 2013. Phenological versus meteorological controls on land-atmosphere water and carbon fluxes. J. Geophys. Res. Biogeosci. 118, 14–29.
Reed, B.C., Brown, J.F., Vanderzee, D., Loveland, T.R., Merchant, J.W., Ohlen, D.O., 1994. Measuring phenological variability from satellite imagery. J. Veg. Sci. 5, 703–714.
Richardson, A.D., Hollinger, D.Y., Dail, D.B., Lee, J.T., Munger, J.W., O'Keefe, J., 2009. Influence of spring phenology on seasonal and annual carbon balance in two contrasting New England forests. Tree Physiol. 29, 321–331.
Richardson, A.D., Keenan, T.F., Migliavacca, M., Ryu, Y., Sonnentag, O., Toomey, M., 2013. Climate change, phenology, and phenological control of vegetation feedbacks to the climate system. Agric. For. Meteorol. 169, 156–173.
Rocha, A.V., Shaver, G.R., 2009. Advantages of a two band EVI calculated from solar and photosynthetically active radiation fluxes. Agric. For. Meteorol. 149, 1560–1563.
Román, M.O., Csiszar, I., Justice, C., Key, J., Privette, J., Devadiga, S., Davidson, C., Wolfe, R.E., Masuoka, E.J., 2012. Status of the Suomi NPP visible/infrared imager radiometer suite's (VIIRS) land environmental data records (EDRs) after early evaluation of on-orbit performance, paper presented at Geoscience and Remote Sensing Symposium (IGARSS). 2012 IEEE International, pp. 22–27 (July 2012).
Rosemartin, A.H., Denny, E.G., Weltzin, J.F., Marsh, R.L., Wilson, B.E., Mehdipoor, H., Zurita-Milla, R., Schwartz, M.D., 2015. Lilac and honeysuckle phenology data 1956–2014. Sci. Data 2.
Schaaf, C.B., Gao, F., Strahler, A.H., Lucht, W., Li, X.W., Tsang, T., Strugnell, N.C., Zhang, X.Y., Jin, Y.F., Muller, J.P., Lewis, P., Barnsley, M., Hobson, P., Disney, M., Roberts, G., Dunderdale, M., Doll, C., d'Entremont, R.P., Hu, B.X., Liang, S.L., Privette, J.L., Roy, D., 2002. First operational BRDF, albedo nadir reflectance products from MODIS. Remote Sens. Environ. 83, 135–148.
Schaaf, C.B., Liu, J., Gao, F., Strahler, A.H., 2011. MODIS albedo and reflectance an isotropy products from Aqua and Terra. In: Ramachandran, B., Justice, C., Abrams, M. (Eds.), Land Remote Sensing and Global Environmental Change: NASA's Earth Observing System and the Science of ASTER and MODIS. Springer-Cerlag, pp. 549–562.
Tan, B., Morisette, J.T., Wolfe, R.E., Gao, F., Ederer, G.A., Nightingale, J., Pedelty, J.A., 2011. An enhanced TIMESAT algorithm for estimating vegetation phenology metrics from MODIS data. IEEE J. Sel. Top. Appl. Earth Obs. Remote Sens. 4, 361–371.
USGCRP, 2010. Ecosystem responses to climate change: selecting indicators and integrating observational networks. In: NCA Report Series, 5a. Washington, DC, . http://data.globalchange.gov/assets/68/23/2165abcb9561c165fb65ec2dcf3a/ecological-indicators-workshop-report.pdf.
USGCRP, 2015. National Climate Assessment & Development Advisory Committee (2011–2014) Meetings, Decisions, and Adopted Documents. http://www.globalchange.gov/what-we-do/assessment/ncadac.
Vargas, M., Miura, T., Shabanov, N., Kato, A., 2013. An initial assessment of Suomi NPP VIIRS vegetation index EDR. J. Geophys. Res.-Atmos. 118, 12301–12316.
Vina, A., Henebry, G.M., Gitelson, A.A., 2004. Satellite monitoring of vegetation dynamics: sensitivity enhancement by the wide dynamic range vegetation index. Geophys. Res. Lett. 31.
Vivoni, E.R., 2012. Diagnosing seasonal vegetation impacts on evapotranspiration and its partitioning at the catchment scale during SMEX04-NAME. J. Hydrometeorol. 13, 1631–1638.
Walther, G.R., 2010. Community and ecosystem responses to recent climate change. Philos. Trans. R. Soc. B 365, 2019–2024.
Wang, Z.S., Schaaf, C.B., Chopping, M.J., Strahler, A.H., Wang, J.D., Roman, M.O., Rocha, A.V., Woodcock, C.E., Shuai, Y.M., 2012. Evaluation of Moderate-resolution Imaging Spectroradiometer (MODIS) snow albedo product (MCD43A) over tundra. Remote Sens. Environ. 117, 264–280.
Wang, Z.S., Schaaf, C.B., Sun, Q.S., Kim, J., Erb, A.M., Gao, F., Roman, M.O., Yang, Y., Petroy, S., Taylor, J.R., Masek, J.G., Morisette, J.T., Zhang, X.Y., Papuga, S.A., 2017. Monitoring land surface albedo and vegetation dynamics using high spatial and temporal resolution synthetic time series from Landsat and the MODIS BRDF/NBAR/albedo product. Int. J. Appl. Earth Obs. Geoinf. 59, 104–117.
Wang, Z., Schaaf, C.B., Sun, Q., Shuai, Y., Román, M.O., 2018. Capturing rapid land

surface dynamics with collection V006 MODIS BRDF/NBAR/albedo (MCD43) products. Remote Sens. Environ. 207, 50–64.
White, M.A., Thornton, P.E., Running, S.W., 1997. A continental phenology model for monitoring vegetation responses to interannual climatic variability. Glob. Biogeochem. Cycles 11, 217–234.
White, M.A., de Beurs, K.M., Didan, K., Inouye, D.W., Richardson, A.D., Jensen, O.P., O'Keefe, J., Zhang, G., Nemani, R.R., van Leeuwen, W.J.D., Brown, J.F., de Wit, A., Schaepman, M., Lin, X.M., Dettinger, M., Bailey, A.S., Kimball, J., Schwartz, M.D., Baldocchi, D.D., Lee, J.T., Lauenroth, W.K., 2009. Intercomparison, interpretation, and assessment of spring phenology in North America estimated from remote sensing for 1982–2006. Glob. Chang. Biol. 15, 2335–2359.
White, K., Pontius, J., Schaberg, P., 2014. Remote sensing of spring phenology in northeastern forests: a comparison of methods, field metrics and sources of uncertainty. Remote Sens. Environ. 148, 97–107.
Williamson, S.N., Barrio, I.C., Hik, D.S., Gamon, J.A., 2016. Phenology and species determine growing-season albedo increase at the altitudinal limit of shrub growth in the sub-Arctic. Glob. Chang. Biol. 22, 3621–3631.
Willmott, C.J., 1981. On the validation of models. Phys. Geogr. 2, 184–194.
Wu, C.Y., Gonsamo, A., Gough, C.M., Chen, J.M., Xu, S.G., 2014. Modeling growing season phenology in North American forests using seasonal mean vegetation indices from MODIS. Remote Sens. Environ. 147, 79–88.
Zhang, X.Y., 2015. Reconstruction of a complete global time series of daily vegetation index trajectory from long-term AVHRR data. Remote Sens. Environ. 156, 457–472.
Zhang, X.Y., Goldberg, M.D., 2011. Monitoring fall foliage coloration dynamics using time-series satellite data. Remote Sens. Environ. 115, 382–391.
Zhang, X.Y., Friedl, M.A., Schaaf, C.B., Strahler, A.H., Hodges, J.C.F., Gao, F., Reed, B.C., Huete, A., 2003. Monitoring vegetation phenology using MODIS. Remote Sens. Environ. 84, 471–475.
Zhang, Q.Y., Xiao, X.M., Braswell, B., Linder, E., Baret, F., Moore, B., 2005. Estimating light absorption by chlorophyll, leaf and canopy in a deciduous broadleaf forest using MODIS data and a radiative transfer model. Remote Sens. Environ. 99, 357–371.
Zhang, X.Y., Friedl, M.A., Schaaf, C.B., 2006. Global vegetation phenology from Moderate Resolution Imaging Spectroradiometer (MODIS): evaluation of global patterns and comparison with in situ measurements. J. Geophys. Res. Biogeosci. 111.
Zhang, X.Y., Tarpley, D., Sullivan, J.T., 2007. Diverse responses of vegetation phenology to a warming climate. Geophys. Res. Lett. 34.
Zhang, Q.Y., Middleton, E.M., Margolis, H.A., Drolet, G.G., Barr, A.A., Black, T.A., 2009. Can a satellite-derived estimate of the fraction of PAR absorbed by chlorophyll (FAPAR(chl)) improve predictions of light-use efficiency and ecosystem photosynthesis for a boreal aspen forest? Remote Sens. Environ. 113, 880–888.
Zhang, X.Y., Friedl, M., Schaaf, C., 2009. Sensitivity of vegetation phenology detection to the temporal resolution of satellite data. Int. J. Remote Sens. 30, 2061–2074.
Zhang, X.Y., Tan, B., Yu, Y.Y., 2014. Interannual variations and trends in global land surface phenology derived from enhanced vegetation index during 1982–2010. Int. J. Biometeorol. 58, 547–564.
Zhang, X.Y., Friedl, M.A., Henebry, G.M., Schaaf, C., Miura, T., 2017a. VIIRS global land surface phenology product user guide, version 1.0. https://viirsland.gsfc.nasa.gov/PDF/GLSP-UserM_V1.0_draft_July2017.pdf.
Zhang, X.Y., Liu, L.L., Yan, D., 2017b. Comparisons of global land surface seasonality and phenology derived from AVHRR, MODIS, and VIIRS data. J. Geophys. Res. Biogeosci. 122, 1506–1525.
Zhang, X.Y., Wang, J.M., Gao, F., Liu, Y., Schaaf, C., Friedl, M., Yu, Y.Y., Jayavelu, S., Gray, J., Liu, L.L., Yan, D., Henebry, G.M., 2017c. Exploration of scaling effects on coarse resolution land surface phenology. Remote Sens. Environ. 190, 318–330.
Zhang, X.Y., Jayavelu, S., Liu, L.L., Friedl, A.M., Henebry, G.M., Liu, Y., Schaaf, C., Richardson, A.D., Gray, J., 2018. Evaluation of land surface phenology from VIIRS data using time series of PhenoCam imagery. Agric. For. Meteorol. 256-257, 137–149.